Regulation of mammalian siderophore 2,5-DHBA in the innate immune response to infection

Zhuoming Liu,[1,2] Scott Reba,[3] Wei-Dong Chen,[5] Suheel Kumar Porwal,[1,2] W. Henry Boom,[3] Robert B. Petersen,[2] Roxana Rojas,[3] Rajesh Viswanathan,[4] and L. Devireddy[1,2]

[1]Case Comprehensive Cancer Center; [2]Department of Pathology; [3]Department of Medicine, Tuberculosis Research Institute and Division of Infectious Diseases; and [4]Department of Chemistry, Case Western Reserve University, Cleveland, OH 44106
[5]Genetics Branch , National Cancer Institute/National Institutes of Health, Bethesda, MD 20892

Competition for iron influences host–pathogen interactions. Pathogens secrete small iron-binding moieties, siderophores, to acquire host iron. In response, the host secretes siderophore-binding proteins, such as lipocalin 24p3, which limit siderophore-mediated iron import into bacteria. Mammals produce 2,5-dihydroxy benzoic acid, a compound that resembles a bacterial siderophore. Our data suggest that bacteria use both mammalian and bacterial siderophores. In support of this idea, supplementation with mammalian siderophore enhances bacterial growth in vitro. In addition, mice lacking the mammalian siderophore resist *E. coli* infection. Finally, we show that the host responds to infection by suppressing siderophore synthesis while up-regulating lipocalin 24p3 expression via TLR signaling. Thus, reciprocal regulation of 24p3 and mammalian siderophore is a protective mechanism limiting microbial access to iron.

CORRESPONDENCE
L. Devireddy:
lxd59@case.edu

Abbreviations used: BDH2 3-OH, butyrate dehydrogenase-2; BLIMP-1, B lymphocyte-induced maturation protein-1; DHBA, dihydroxy benzoic acid; FepA, ferric enterobactin receptor; GC-MS, gas chromatography mass spectrometry; HSD, honestly significant difference.

The growth and metabolism of many pathogenic microbes is exquisitely iron sensitive (Schaible and Kaufmann, 2004). Mammals have evolved a defense mechanism to sequester iron that permits host cells to maintain access to iron while preventing invading microbes from acquiring the metal (Ganz, 2009; Cassat and Skaar, 2013). Iron is predominantly intracellular or tightly bound to proteins. Invading pathogens therefore obtain iron from their host by secreting small, iron-binding siderophores, which remove iron from host protein–iron complexes due to their higher affinity for iron (Miethke and Marahiel, 2007). In parallel, mammals have evolved siderophore-binding proteins as components of the innate immune system, e.g., 24p3 (Flo et al., 2004). 24p3 is a member of the lipocalin family of proteins that transport a variety of ligands (Flower, 2000). 24p3 binds small hydrophobic molecules, the siderophores (Goetz et al., 2002). By binding iron-laden bacterial siderophores, 24p3 participates in innate host defense (Flo et al., 2004; Berger et al., 2006; Saiga et al., 2008). 24p3 expression in innate immunity is highly induced in response to stimulation by TLR2, TLR4, and TLR5 agonists (Flo et al., 2004; Saiga et al., 2008; Van Maele et al., 2010). 24p3 is also one of the secondary granule proteins of neutrophils (Kjeldsen et al., 1993). Therefore, the 24p3 released upon neutrophil degranulation, complements 24p3 secreted by TLR stimulated macrophages, epithelial cells and liver opposing salvage of host iron by bacterial siderophores (Borregaard and Cowland, 2006).

24p3 specifically binds catecholate or mixed phenolate type siderophores (Holmes et al., 2005). The ability of 24p3 to curtail the growth of bacteria is limited to those species that depend on catecholes and mixed phenolates for iron acquisition (Berger et al., 2006, Flo et al., 2004; Saiga et al., 2008). Strains of *E. coli* and *Staphylococcus aureus* have modified siderophores that evade capture by 24p3 (Fischbach et al., 2006). Moreover, pathogenic strains of *E. coli* secrete multiple siderophores (Henderson et al., 2009). Although 24p3 is highly induced by infection with these

The Rockefeller University Press $30.00
J. Exp. Med. 2014 Vol. 211 No. 6 1197-1213
www.jem.org/cgi/doi/10.1084/jem.20132629

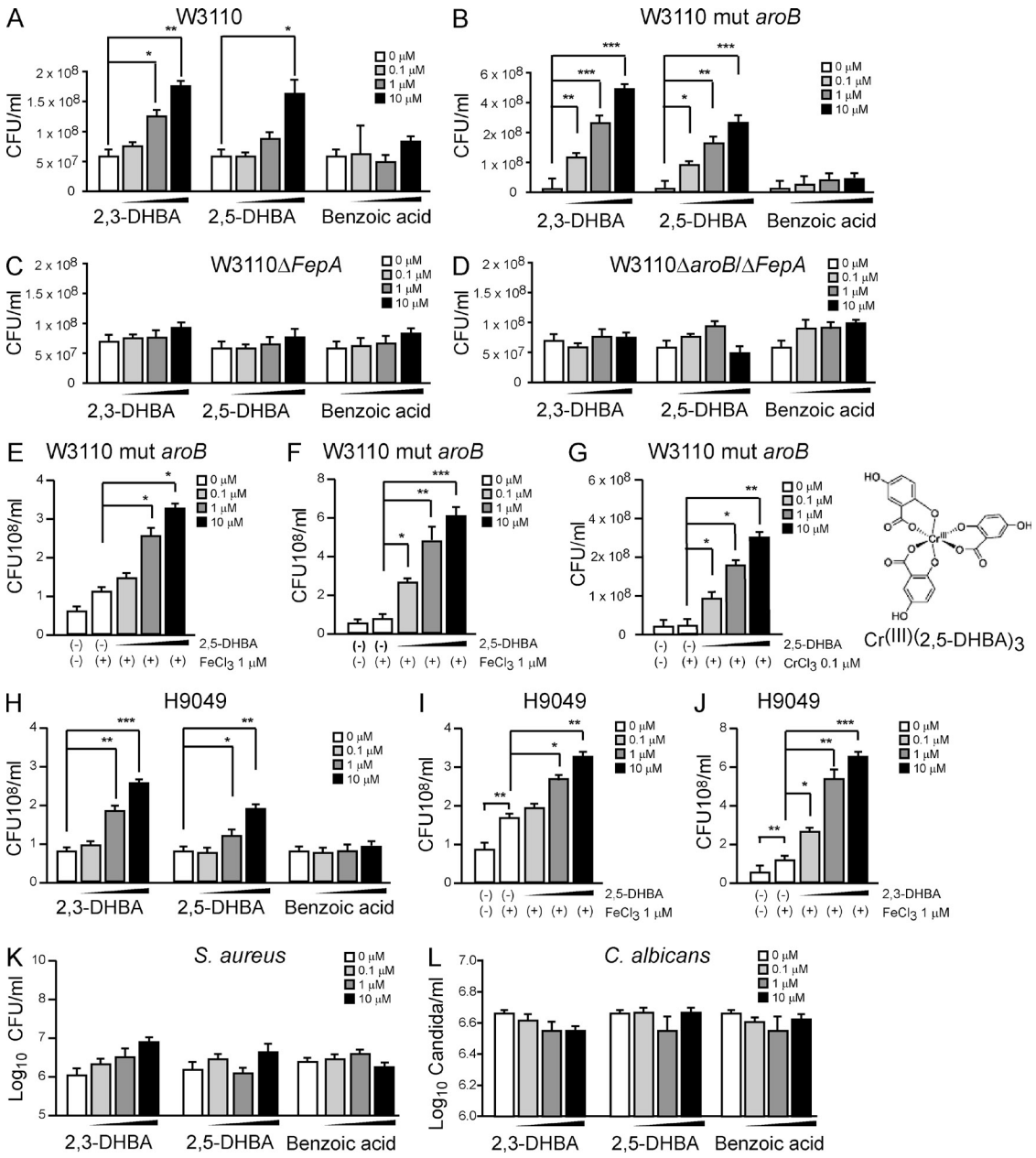

Figure 1. 2,5-DHBA-mediated growth augmentation of *E. coli* in vitro. (A–D) *E. coli* W3110 (A), *E. coli* W3110 mut *aroB* (B), *E. coli* W3110Δ*FepA* (C) or *E. coli* W3110Δ*FepA*/Δ*aroB* (D; 10^4 CFU/ml each) was cultured in the presence of the indicated amounts of 2,5-DHBA, 2,3-DHBA, or benzoic acid overnight and CFU were determined at 12 h after culture. Data are the means of three independent experiments ± SD. Statistical analysis by one-way analysis of variance followed by the Tukey HSD test for multiple comparisons: *, $P < 0.05$; **, $P < 0.01$, ***, $P < 0.001$. (E and F) *E. coli* W3110 mut a*roB* (10^4 CFU/ml) was cultured in the presence of 0.1 μM $FeCl_3$ and increasing concentrations of 2,5-DHBA (E) or 2,3-DHBA (F) overnight and CFU were determined at 12 h after culture. Data are the means of three independent experiments ± SD. Statistical analysis by one-way analysis of variance followed by the Tukey HSD test for multiple comparisons: *, $P < 0.05$; **, $P < 0.01$; ***, $P < 0.001$. (G, right) Schematic showing chromium substitution in 2,5-DHBA. (left) *E. coli* W3110 mut a*roB* (10^4 CFU/ml) was cultured in the presence of 0.1 μM $CrCl_3$ and increasing concentrations of 2,5-DHBA overnight and CFU were determined at 12 h after culture. Data are the means of three independent experiments ± SD. Statistical analysis by one-way analysis of variance followed by the Tukey HSD test for multiple comparisons: *, $P < 0.05$; **, $P < 0.01$. (H) *E. coli* H9049 (10^4 CFU/ml) was cultured as stated in A. Statistical analysis by one-way analysis of variance followed by the Tukey HSD test for multiple comparisons: *, $P < 0.05$; **, $P < 0.01$; ***, $P < 0.001$. (I and J) *E. coli* H9049 (10^4 CFU/ml) was cultured in the presence of 0.1 μM $FeCl_3$ and increasing concentrations of 2,5-DHBA (H) or 2,3-DHBA (I) and CFU were determined 12 h after culture. Data are the means of three independent experiments ± SD. Statistical analysis by one-way analysis of variance followed by the Tukey HSD test for multiple comparisons: *, $P < 0.05$; **, $P < 0.01$; ***, $P < 0.001$. (K) DHBA supplementation has no effect on *S. aureus* growth. *S. aureus* strain 25923 at 10^5 CFU/ml was cultured in the presence of indicated amounts of 2,5-DHBA, 2,3-DHBA, or benzoic acid overnight and CFU were determined at 12 h after culture by plating onto tryptic soy agar plates. Data are the means of three independent experiments ± SD. Statistical analysis by

bacteria, secreted 24p3 may not be able to sequester the multiple siderophores excreted by these bacteria because its binding pocket is selective for catecholes (Holmes et al., 2005; Reigstad et al., 2007). Interestingly, 24p3 is also highly induced by *E. coli* infection of C3H/HeJ mice that harbor a mutation in TLR4 (Reigstad et al., 2007). Despite high levels of 24p3, these mice succumb to *E. coli* infection; the effect of 24p3 on *E. coli* growth in C3H/HeJ mice is insignificant (Hagberg et al., 1985). As stated above, 24p3 is a secondary granule protein in neutrophils, which is critical for motility and chemotaxis (Rathore et al., 2011; Schroll et al., 2012; Liu et al., 2013). 24p3 deficiency confers enhanced sensitivity upon mice to a variety of pathogens independent of their ability to secrete siderophores (Liu et al., 2013). These studies suggest that additional mechanisms may be in place that synergize with 24p3 to counter bacterial hijacking of iron.

Mammalian-derived 24p3 also captures iron indicating the existence of siderophore-like molecules (Yang et al., 2003). In addition, older studies have suggested the existence of low-molecular weight iron binding compounds or siderophore-like molecules that are capable of binding iron and that stimulate proliferation of bacteria (Fernandez-Pol, 1978; Jones et al., 1980). However, these molecules were not implicated in iron carrier function of 24p3. Using 24p3 as bait we recently identified a siderophore in mammalian cells that facilitates iron loading onto 24p3 (Devireddy et al., 2010). The mammalian siderophore, 2,5-dihydroxy benzoic acid (2,5-DHBA) is chemically similar to 2,3-DHBA, the iron-binding moiety of *E. coli* enterobactin (Raymond et al., 2003). One of the short chain dehydrogenases (SDR) family of reductases, 3-OH butyrate dehydrogenase-2 (Bdh2), a homologue of bacterial EntA, catalyzes a rate-limiting step in the 2,5-dihydroxy benzoic acid (DHBA) biosynthetic pathway (Devireddy et al., 2010).

However, the role of the mammalian siderophore in innate immunity is not clear. Due to its similarity to bacterial siderophore, we hypothesized that the mammalian siderophore promotes bacterial growth. We now show that the mammalian siderophore augments bacterial growth and can rescue a growth deficit conferred by the absence of the *E. coli* siderophore, enterobactin. To counter bacterial coopting of the mammalian siderophore, the host responds by suppressing mammalian siderophore biosynthesis. Thus, negative regulation of the mammalian siderophore provides an ingenious strategy to withhold iron from invading pathogens. Of note, mammalian siderophore-deficient mice resist pathogenic *E. coli*. In addition to decreasing mammalian siderophore the host responds by secreting 24p3 to sequester iron-laden bacterial siderophores. Thus, reciprocal regulation of 24p3 and the mammalian siderophore restricts the growth of invading pathogens.

RESULTS

2,5–DHBA, the mammalian siderophore augments bacterial growth in vitro

Previously, both 2,3-DHBA and enterobactin were shown to confer a growth advantage to *E. coli* by promoting iron uptake (Hancock et al., 1977). The mammalian siderophore, 2,5-DHBA, resembles 2,3-DHBA, so we reasoned that 2,5-DHBA may also promote bacterial growth. We tested this hypothesis using an *E. coli* strain harboring a mutation in the *aroB* gene (W3110 mut *aroB*) whose gene product catalyzes one of the early steps in the shikimate pathway preventing enterobactin synthesis (Braun et al., 1983; Chaudhuri et al., 1986; Bentley, 1990). In iron-restrictive medium (RPMI), the *aroB* mutant grows poorly compared with the parental *E. coli* W3110 strain (Braun et al., 1983). As expected, addition of 2,3-DHBA augmented growth of the *aroB* mutant (Fig. 1 B). The growth promoting activity of 2,3-DHBA on the *aroB* mutant is less effective than that observed in parental *E. coli* W3110 (Fig. 1 A). However, 2,5-DHBA also augmented the growth of the *aroB* mutant in a dose-dependent manner (Fig. 1 B). Supplementation with 2,5-DHBA augmented the growth of parental W3110 strain, although less efficiently than 2,3-DHBA (Fig. 1 A). In contrast, addition of benzoic acid, a chemical paralogue of 2,5-DHBA, had a minimal effect on the growth of both parental or *aroB* mutant *E. coli* strains (Fig. 1 B). Thus, supplementation with 2,5-DHBA rescues the growth deficit caused by the absence of enterobactin.

The enterobactin receptor, FepA, facilitates iron import mediated by both 2,3-DHBA and enterobactin (Barnard et al., 2001). To determine whether FepA mediates 2,5-DHBA growth promotion we used an *E. coli* strain lacking *fepA* (Vakharia and Postle, 2002). The *fepA* deletion strain grew poorly in iron-limiting medium compared with the parental W3110 strain (not depicted). Addition of either 2,3-DHBA or 2,5-DHBA failed to augment the growth of the *fepA* deletion strain (Fig. 1 C; Bleuel et al., 2005). However, addition of 2,3-DHBA or 2,5-DHBA readily promoted the growth of parental W3110 strain (Fig. 1 A). These results suggest that both molecules use a common transport pathway (Fig. 1 C).

Finally, we tested the effect of 2,5-DHBA on an *E. coli* strain bearing deletions in both *fepA* and *aroB* genes (Vakharia and Postle, 2002). The double deletion strain grew very poorly in iron-limiting medium when compared with parental W3110 strain (not depicted). Addition of 2,5-DHBA or 2,3-DHBA failed to confer a growth advantage to the double deletion strain (Fig. 1 D). Therefore, the 2,5-DHBA–mediated growth advantage requires FepA.

Both 2,3-DHBA and 2,5-DHBA chelate ferric iron (Albrecht-Gary and Crumbliss, 1998; Devireddy et al., 2010). Therefore, the observed growth promoting effect of these

one-way analysis of variance followed by the Tukey HSD test for multiple comparisons. $P < 0.05$ was considered significant. (L) *C. albicans* is impervious to DHBA supplementation. *C. albicans* strain 562 at 10^6 CFU/ml was cultured in the presence of indicated amounts of 2,5-DHBA, 2,3-DHBA, or benzoic acid overnight and their number was enumerated in a hemocytometer 24 h after culture. Data are the means of three independent experiments ± SD. Statistical analysis by one-way analysis of variance, followed by the Tukey HSD test for multiple comparisons. $P < 0.05$ was considered significant.

two molecules may result from enhanced uptake of iron mediated by 2,3-DHBA or 2,5-DHBA. We assessed growth rates of the *aroB* mutant under iron-replete condition with or without 2,5-DHBA and, as a control, 2,3-DHBA to test this idea (Fig. 1, E and F). Exogenous supplementation with ferric iron alone conferred a marginal growth advantage when compared with medium alone (Fig. 1, E and F). However, addition of iron complexed with 2,5-DHBA or 2,3-DHBA substantially enhanced the growth of the *aroB* mutant strain (Fig. 1, E and F). Radiolabeled iron uptake experiments with or without 2,5-DHBA or 2,3-DHBA or benzoic acid as a control confirmed this result (unpublished data). Substitution of iron with chromium (another *d*-block transition metal) in the 2,5-DHBA–ferric iron complex did not further enhance the growth of the *aroB* mutant (Fig. 1 G). These results suggest that 2,5-DHBA confers a growth advantage on the *aroB* mutant by facilitating iron uptake.

To generalize of these results, we evaluated the growth-promoting activity of 2,5-DHBA on pathogenic bacteria (virulent *E. coli* strain H9049 [Flo et al., 2004] and *S. aureus* strain 25923) and pathogenic yeast (*Candida albicans* strain 562). Addition of 2,5-DHBA augmented the growth of *E. coli* strain H9049 (Fig. 1 H), whereas addition of benzoic acid had no effect (Fig. 1 H). As expected, addition of 2,3-DHBA also augmented growth (Fig. 1 H). We next assessed *E. coli* H9049 strain growth under iron-replete conditions with or without 2,5-DHBA or 2,3-DHBA as a positive control. Exogenous supplementation with ferric iron conferred a marginal growth advantage (Fig. 1, I and J). However, addition of 2,5-DHBA or 2,3-DHBA in the presence of ferric iron significantly enhanced *E. coli* H9049 growth compared with iron or 2,5-DHBA alone (Fig. 1, I and J). Collectively, these results suggest that 2,5-DHBA promotes *E. coli* growth by facilitating iron acquisition.

In contrast to *E. coli*, we found that addition of 2,5-DHBA had no effect on the growth of *S. aureus* (Fig. 1 K). Similarly, addition of 2,3-DHBA or enterobactin had no effect on the growth of *S. aureus* (Fig. 1 K). Supplementation with 2,3-DHBA or 2,5-DHBA also failed to significantly affect the growth of pathogenic *C. albicans* (Fig. 1 L). *C. albicans* lack FepA, which is required for 2,3-DHBA– or 2,5-DHBA–mediated growth augmentation (Fig. 1; Almeida et al., 2009). In contrast, *S. aureus* expresses FepA but is unable to import ferric enterobactin (Fig. 1; Turlin et al., 2013), thus limiting growth promotion by either compound.

In summary, 2,5-DHBA specifically promotes *E. coli* growth by facilitating iron acquisition, and the growth-promoting effect of 2,5-DHBA is similar to that observed with 2,3-DHBA.

Derivation of 2,5-DHBA deficient mice

To test the role of the mammalian siderophore on bacterial growth in vivo, we generated mice lacking Bdh2 activity. The catalytic activity of Bdh2 is dependent on NPG and SYK motifs, which are encoded by *exon* 7 (Guo et al., 2006). We replaced *exon* 7 of the *bdh2* gene with a *neomycin* resistance cassette (Fig. 2 A). By interbreeding *bdh2* heterozygous mice, we obtained nearly 25% *bdh2*-null mice suggesting that the *bdh2* deletion did not affect the viability of the embryos.

The mutant mice are slightly runted but otherwise grossly indistinguishable from their normal counterparts when housed in specific pathogen–free conditions and fed standard laboratory diet (Prolab RMH3000) containing 0.02% wt/wt iron. However, when placed on a low-iron diet (TD.80396; containing 0.0006% wt/wt iron and 0.001% wt/wt ethoxyquin) the mutant mice exhibited severe anemia, alopecia, and hypothermia. Challenge with a high-iron diet (TD.08496; containing 2% wt/wt carbonyl iron and 0.001% wt/wt ethoxyquin) led to premature mortality, growth retardation, and extreme iron overload (unpublished data).

Bdh2-null mice have no detectable 2,5-DHBA

We previously demonstrated that suppression of Bdh2 results in depletion of 2,5-DHBA in cultured cells (Devireddy et al., 2010). We next asked whether *bdh2* deletion in mice abrogates 2,5-DHBA synthesis. We assessed levels of 2,5-DHBA in urine samples collected from WT and *bdh2*-null mice by gas chromatography-mass spectrometry (GC-MS) analysis. A prominent GC peak was detected at 7.2 s retention time representing 2,5-DHBA in WT urine sample (Fig. 2 B). The presence of 2,5-DHBA in urine sample from WT mice was further confirmed using a set of DHBA standards (Fig. 2 B). In addition to 2,5-DHBA, we also found several DHBA-like molecules in the WT urine sample (Fig. 2 B). In contrast, urine from *bdh2*-null mice lack 2,5-DHBA reinforcing the notion that Bdh2 catalyzes the synthesis of 2,5-DHBA (Fig. 2 B).

Disruption of bdh2 does not alter ketone body metabolism

An earlier study suggested a role for BDH2 in ketone body metabolism. Based on a computational model, Bdh2 was assumed to bind and oxidize cytosolic ketone bodies (Guo et al., 2006). Therefore, we evaluated levels of ketone bodies in plasma samples obtained from WT and *bdh2*-null mice, specifically 3 hydroxybutyric acid, the most abundant ketone in the body. WT mice displayed basal levels of 3 hydroxybutyric acid (Fig. 2 C). Surprisingly, 3 hydroxybutyric acid levels in *bdh2*-null mice were comparable to WT mice (Fig. 2 C). Further evaluation of acetoacetate also suggested no ketoacidosis in *bdh2*-null mice (Fig. 2 D).

In mammals, ketone bodies are derived from the oxidation of fatty acids that are then exported to other tissues to be used as fuel (Cotter et al., 2013). Therefore, we assessed cholesterol, free fatty acids (FFA), and triglyceride levels in plasma samples from WT and *bdh2*-null mice. Plasma fatty acid levels were unremarkable in *bdh2*-null mice compared with the levels in WT mice (Fig. 2, E–G). In addition, because glucose metabolism and ketone body oxidation are linked, we assessed glucose handling in *bdh2*-null mice after overnight fasting. No significant difference was observed between WT and *bdh2*-null mice (unpublished data). Thus, Bdh2 deficiency does not appear to impair ketone body metabolism.

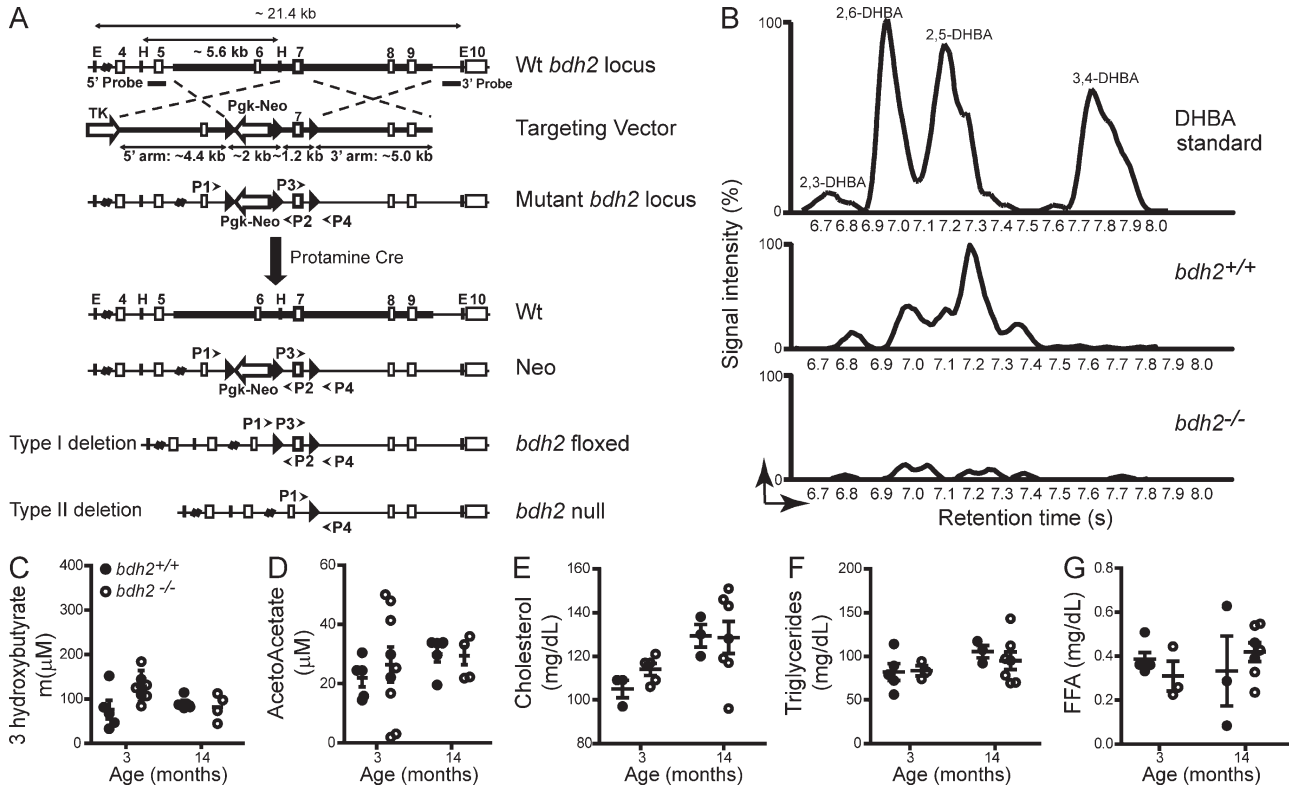

Figure 2. Derivation of *bdh2* knockout mice. (A) Schematic representation of the targeting strategy and the expected patterns of Cre-mediated homologous recombination. The structure of the *bdh2* locus is shown at the top, the targeting construct in the middle and the resulting targeted allele at the bottom. Numbered boxes indicate *exons*. Black triangles indicate *LoxP* sites. Arrowheads indicate PCR primer locations for genotyping (P1-P4). 5′ and 3′ external probes indicated by solid lines. *TK*, herpes simplex virus thymidine kinase gene. Restriction sites, HindIII (H), EcoRI (E), used for Southern blot genotyping are indicated. (B) Assessment of 2,5-DHBA levels in urine samples of control and *bdh2*-null mice. A total of 10 age- and sex-matched WT and *bdh2*-null mice on C57BL/6 genetic background were analyzed. Representative GC-MS spectra of the TMS-derivatized, small molecule fractions from urine specimen from WT and *bdh2*-null mice were shown. A set of DHBA standards is shown on the top. (C and D) Bdh2 deficiency does not alter ketone body metabolism. Measurement of 3-hydroxybutyrate and acetoacetate levels in plasma of 8-wk-old female WT and *bdh2*-null mice on C57BL/6 genetic background. Data are representative of two independent experiments, each with at least 4–9 mice per group. Statistical analysis by one-way analysis of variance followed by the Tukey HSD test for multiple comparisons. $P < 0.05$ was considered significant. (E–G) Evaluation of fatty acid profiles in plasma of 8-wk-old female WT and *bdh2*-null mice on C57BL/6 genetic background. Data are representative of two independent experiments, each with at least 4–9 mice per group. Statistical analysis by one-way analysis of variance followed by the Tukey HSD test for multiple comparisons. $P < 0.05$ was considered significant.

Siderophore-deficient mice are resistant to bacterial infection

To test whether 2,5-DHBA–deficient mice resist *E. coli* infection, we challenged *bdh2*-null mice with an acute lethal dose of a clinical strain of *E. coli*, H9049. As in earlier studies (Flo et al., 2004), low doses ($<1.5 \times 10^8$ CFU) did not impair the survival of WT mice (unpublished data). However, a higher dose (2.5×10^8 CFU), resulted in 100% death of the WT mice by 24 h compared with 60% of *bdh2*-null mice (Fig. 3 A). 40% of the *bdh2*-null mice went on to recover from infection; none of the WT mice survived (Fig. 3 A). Additionally, the bacterial burden was lower when compared with WT mice (Fig. 3, C–E).

The *E. coli* H9049 strain secretes only enterobactin for iron acquisition (Flo et al., 2004), whereas most pathogenic *E. coli* secrete more than one siderophore (Henderson et al., 2009). To determine whether the observed resistance to *E. coli* H9049 applies to other pathogenic *E. coli* we used the *E. coli* 25922 strain, which secretes both enterobactin and aerobactin (Berger et al., 2006). 2,5-DHBA deficiency also conferred resistance to *E. coli* 25922 challenge, supporting the generality of resistance to bacterial infections conferred by absence of BDH2 (Fig. 3 B). ∼20% of *E. coli* 25922–infected *bdh2*-null mice recovered from infection, whereas none of the infected WT mice survived (Fig. 3 B). The number of *bdh2*-null mice that recovered from *E. coli* 25922 challenge is lower than the number that recovered from *E. coli* H9049 challenge (Fig. 3, A and B). The difference in recovery may result from the secretion of additional siderophores by *E. coli* 25922 making them less dependent on 2,5-DHBA for iron uptake. Bacterial loads in *E. coli* 25922–infected mice are also lower than in WT mice (unpublished data). The *E. coli* challenge experiments demonstrate that 2,5-DHBA deficiency hampers growth of *E. coli* in vivo and confers resistance to mice.

We found that 2,5-DHBA–mediated *E. coli* growth enhancement requires the presence of FepA. Although *S. aureus* expresses FepA, it is unable to import ferric enterobactin (Turlin et al., 2013). To expand on this finding, we challenged *bdh2*-null mice with *S. aureus* (Fig. 3 F). Although we found that the onset of mortality in *S. aureus*–challenged *bdh2*-null mice is later than in WT mice, the mortality rate was not statistically different (Fig. 3 F). Furthermore, liver bacterial loads in

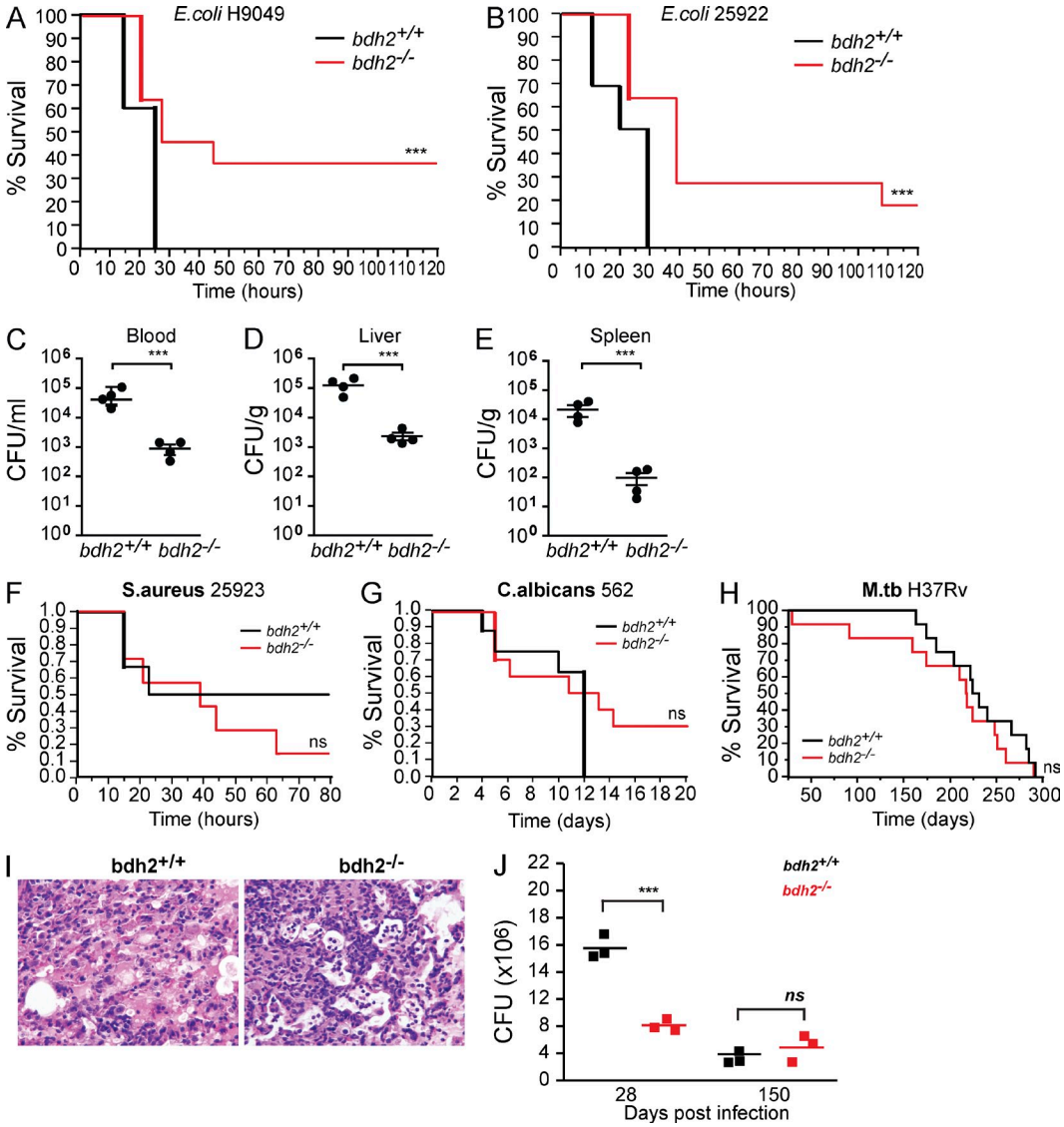

Figure 3. 2,5-DHBA deficient mice are resistant to *E. coli* infection. (A and B) WT and *bdh2*-null mice were infected with 2.5×10^8 CFU of *E. coli* H9049 strain (A) or 10^8 CFU of *E. coli* 25922 strain (B) i.p. and their survival was monitored for 7 d. Data are representative of 2 independent experiments with 8–13 mice per group. Statistical analysis by log-rank test: ***, $P < 0.001$. (C–E) Bacterial loads in blood and parenchymal tissues of WT and *bdh2*-null mice 36 h after infection with 0.6×10^8 CFU of *E. coli* H9049. Blood (C) or homogenates of liver (D) and spleen (E) were plated on LB agar plates and the CFU were determined. Symbols represent individual mice. Bars represent the mean CFU. Data are representative of two independent experiments, each with at least four mice per group. Statistical analysis by two-tailed unpaired Student's *t* test with Welch's correction: ***, $P < 0.001$. (F) Survival curve comparing WT and *bdh2*-null mice after i.p. challenge with *S. aureus* 25923 strain (3×10^8 CFU). Mice were monitored for 4 d after challenge. Data are representative of two independent experiments with seven mice per group. Statistical analysis by log-rank test: ns, not significant. (G) Survival curve comparing WT and *bdh2*-null mice after i.p. challenge with 7×10^7 *C. albicans*. Mice were monitored for 3 wk after challenge. Data are representative of two independent experiments with 10 mice per group. Statistical analysis by log-rank test: ns, not significant. (H) Survival analysis of WT and *bdh2*-null mice infected with *M. tuberculosis* (*M. tb*) H37Rv. Mice were monitored for 300 d after challenge. Each group contained 12 mice. Statistical analysis by log-rank test: ns, not significant. (I) Histological analysis of representative lung sections (H&E) from WT and *bdh2*-null mice infected with *M. tuberculosis* H37Rv. Bars, 100 µM. (J) CFU determination in lung homogenates of WT and *bdh2*-null mice infected with *M. tuberculosis*. Symbols represent individual mouse. Bars represent the mean CFU. Data are representative of two independent experiments, each with at least three mice per group. Statistical analysis by two-tailed unpaired Student's *t* test with Welch's correction: ns, not significant; ***, $P < 0.001$.

S. aureus–challenged WT and *bdh2*-null mice were similar (not depicted). These results show that 2,5-DHBA deficiency does not alter sensitivity to *S. aureus*.

C. albicans does not express FepA and is unaffected by 2,5-DHBA supplementation (Almeida et al., 2009). Based on this observation, we reasoned that *bdh2*-null mice might not display altered sensitivity to *C. albicans*. *Bdh2*-null mice react very similarly to WT mice after *C. albicans* inoculation (Fig. 3 G). As with *S. aureus*, the microbial load in WT and *bdh2*-null mice are comparable (not depicted). Together these results suggest that *bdh2*-null mice are neither sensitive nor resistant to *C. albicans* challenge.

E. coli and *S. aureus* proliferate in the extracellular milieu and cause systemic infection. In contrast, *Mycobacterium tuberculosis* is an intracellular pathogen. To assess the relative resistance of the *bdh2*-null mice to *M. tuberculosis* (strain H37Rv), control, and *bdh2*-null mice were nebulized with *M. tuberculosis* H37Rv and their survival after infection was determined. The onset of mortality in *M.* tuberculosis–challenged *bdh2*-null mice trended earlier than WT mice, but these differences did not achieve significance ($P = 0.29$; Fig. 3 H). The bacterial burden in the lungs of *M. tuberculosis* infected *bdh2*-null mice 4 and 20 wk after infection was initially very low in *bdh2*-null mice as compared with WT mice; however, at later stages of infection, the CFU titers were similar to those observed in WT mice (Fig. 3 J). Histological analysis of lungs of infected WT and *bdh2*-null mice at 28 d after infection revealed changes suggestive of an inflammatory response, which was exacerbated in *bdh2*-null mice (Fig. 3 I). There were no changes in leukocyte parameters in *bdh2*-null mice, suggesting that the observed sensitivity to *M. tuberculosis* was not caused by alterations in leukocyte numbers. These results indicate that 2,5-DHBA deficiency has a limited impact on the pathogenesis of *M. tuberculosis*.

Exogenous supplementation of 2,5-DHBA confers bacterial sensitivity to *bdh2*-null mice

To determine whether exogenous supplementation with 2,5-DHBA alters the course of *E. coli* infection in *bdh2*-null mice, we first assessed the kinetics of 2,5-DHBA absorption, distribution, and clearance using ^{13}C-labeled 2,5-DHBA and mass spectrometry. Fig. 4 A shows the derivation of ^{13}C 2,5-DHBA from ^{13}C salicylic acid. Proton (^{1}H) and ^{13}C NMR analyses were used to assess the purity of the synthesized compound. We injected ^{13}C-2,5-DHBA at 20 μg/kg i.p. and studied the kinetics of clearance by analyzing urine samples collected at 4, 8, 12, 24, 48, 72, and 96 h after injection. By 12 h after injection, half of the initial dose of ^{13}C-2,5-DHBA was cleared from the plasma (Fig. 4 B).

To study the effect of exogenously supplied 2,5-DHBA on bacterial growth in *bdh2*-null mice, we pretreated mice with 2,5-DHBA. Injection of 2,5-DHBA at 20 μg/kg achieves WT urine levels (estimated at 5.8 μM; 0.87 μg ml^{-1}; Fig. 4 C) as judged by MS analysis of urine. Injection of 2,5-DHBA at this dose had a minimal effect on serum iron (Fig. 4, D and E).

Pretreated mice were challenged with *E. coli* H9049 and the bacterial burden was determined. Bacterial loads in untreated *bdh2*-null mice were low when compared with untreated WT mice (Fig. 3, C–E; and Fig. 4 I). However, supplementation with 2,5-DHBA augmented growth of *E. coli* in both WT and *bdh2*-null mice (Fig. 4 I). Significantly, pretreatment with 2,5-DHBA + iron complex enhanced growth of *E. coli* in both WT and *bdh2*-null mice (Fig. 4 I). Under similar experimental conditions, pretreatment with 2,5-DHBA + chromium had no effect on the growth of *E. coli* in control or *bdh2*-null mice (not depicted).

We assessed the survival rates of mice supplemented with either 2,5-DHBA, iron, or 2,5-DHBA + iron (Fig. 4, F–H). We found that 2,5-DHBA or iron supplementation alone to WT or *bdh2*-null mice conferred earlier lethality after *E. coli* infection (Fig. 4, F and H). Moreover, mice supplemented with 2,5-DHBA + iron succumbed to *E. coli* infection even earlier, coincident with the heavy *E. coli* burden in these mice (Fig. 4, G and I). Further, *bdh2*-null mice receiving 2,5-DHBA + iron displayed restored sensitivity to *E. coli*, as judged by 100% mortality 24 h after infection (Fig. 4 G).

In summary, supplementation with 2,5-DHBA reverses the *bdh2*-null phenotype, especially those related to *E. coli* challenge.

Normal cytokine profiles in bdh2-null mice

Cellular iron levels are altered in siderophore-deficient cells (Devireddy et al., 2010) and alterations in cellular iron levels have been shown to modulate cytokine production (Wessling-Resnick, 2010). Therefore we evaluated cytokine levels in WT or *bdh2*-null mice challenged with LPS or *E. coli* strain H9049 to determine the effect of siderophore deficiency. As expected, IL-1β, IL-12b, IL-10, IFN-γ, and TNF were increased in a quantitative real-time PCR assay after LPS or *E. coli* challenge in WT mice (Fig. 5). Surprisingly, *bdh2* deficiency only affected the expression of IFN-γ, under similar conditions (Fig. 5 A). Further, IFN-γ levels were also induced by challenge with PAM3-CSK4, a TLR2 agonist (not depicted). Observation of enhanced IFN-γ in *bdh2*-null mice upon stimulation with TLR ligands is significant because IFN-γ limits the availability of iron in macrophages (Nairz et al., 2008). Thus, differential regulation of IFN-γ in *bdh2*-null mice may aid the host by modulating iron availability in phagocytes limiting bacterial proliferation.

TLR ligands regulate the expression of bdh2

In mammals, distinct combinations of at least 10 toll-like receptors (TLRs) discriminate between a large number of microbial components (Beutler, 2009; Kawai and Akira, 2010). Engagement of TLRs by cognate ligands leads to inflammatory and innate immune responses. Mammalian siderophore-deficient mice are resistant to bacterial infections suggesting that the siderophore participates in the innate immune response. We assessed TLR-mediated mammalian siderophore expression in immune cells by determining levels of *bdh2* mRNA and protein in cultured naive macrophages (RAW264.7), as well as in macrophages stimulated with TLR agonists. As expected, cultured naive macrophages showed abundant transcription of *bdh2* mRNA (Fig. 6 A). However, *bdh2* mRNA was reduced

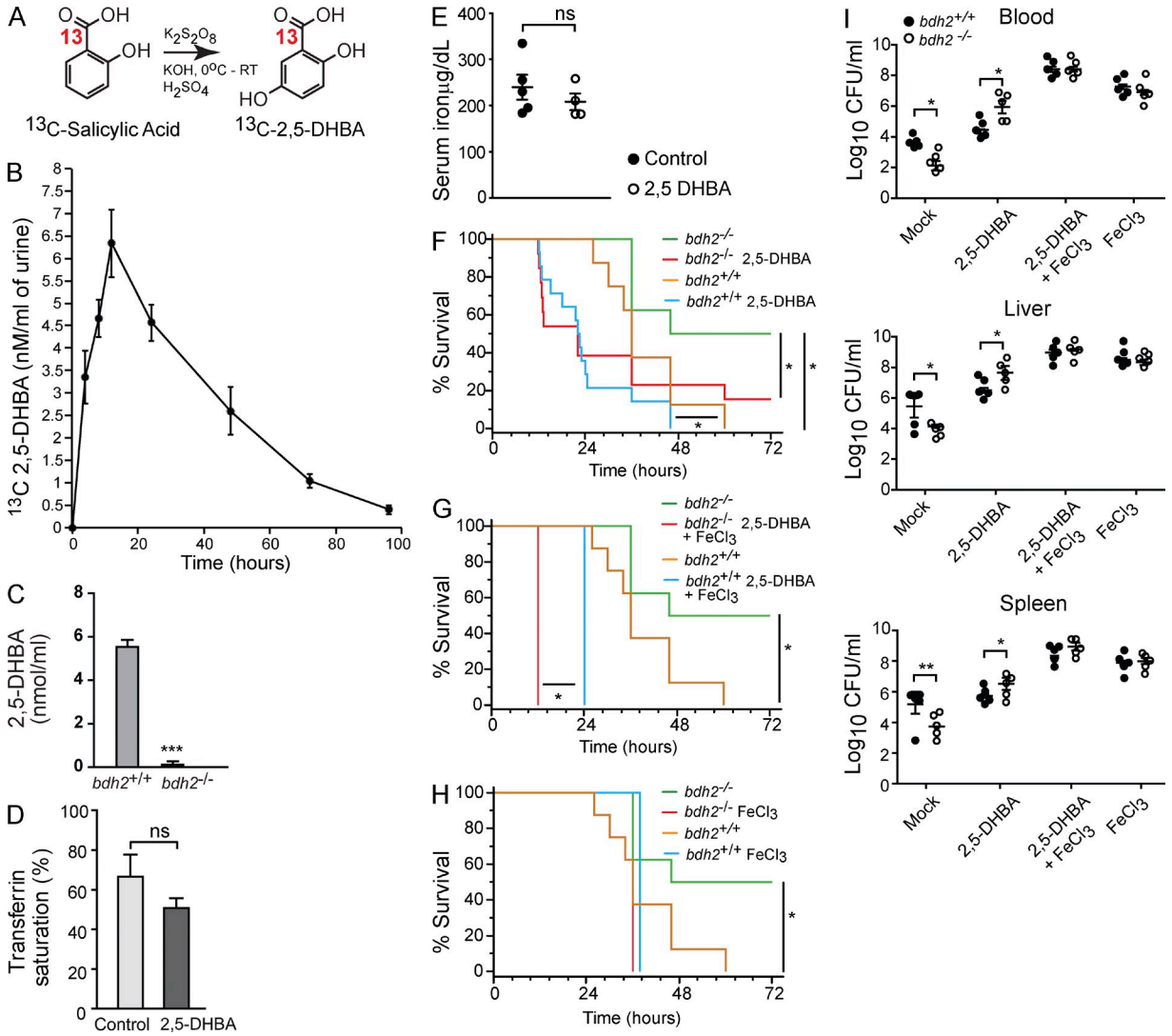

Figure 4. 2,5-DHBA supplementation confers enhanced sensitivity to *E. coli* infection. (A) Schematic representation for derivation of ^{13}C-labeled 2,5-DHBA from ^{13}C salicylic acid. (B) Kinetic analysis of ^{13}C-2,5-DHBA clearance from mice. Mice were injected intraperitoneally with ^{13}C-2,5-DHBA and its elimination from the body was assessed by subjecting urine samples to GC-MS analysis. Data are representative of two independent experiments, each with three mice per group. (C) Quantification of 2,5-DHBA levels in urine samples from control and *bdh2*-null mice. 2,5-DHBA levels were quantitated by comparing to known amounts of 2,5-DHBA. Results show pooled data from two independent experiments, each with at least three mice per group. Statistical analysis by two-tailed unpaired Student's *t* test: ***, $P < 0.001$. (D) Serum transferrin saturation in 8-wk old female C57BL/6 (WT) mice injected with 2,5-DHBA. Results show pooled data from two independent experiments, each with at least three mice per group. Statistical analysis by two-tailed unpaired Student's *t* test: ns, not significant. (E) Iron levels were measured in nonhemolyzed serum of control and 2,5-DHBA–injected mice. Symbols represent individual mice. Bars represent the mean values. Results show pooled data from two independent experiments, each with at least three mice per group. Statistical analysis by two-tailed unpaired *t* test: ns, not significant. (F–H) Survival curve comparing WT and *bdh2*-null mice supplemented with 2,5-DHBA or iron or 2,5-DHBA + iron and challenged with 2×10^8 CFU of *E. coli* H9049 strain. Data are representative of two independent experiments with 4–14 mice per group. Statistical analysis by log-rank test: *, $P < 0.05$. (I) 2,5-DHBA supplementation augments bacterial growth in mice. WT and *bdh2*-null mice were infected with 0.6×10^8 CFU of *E. coli* H9049 strain and bacterial loads in blood and parenchymal tissues after infection were determined. Symbols represent individual mice. Bars represent the mean CFU. Data are representative of two independent experiments, each with at least 5 mice per group. Statistical analysis by two-tailed unpaired Student's *t* test with Welch's correction: *, $P < 0.05$; **, $P < 0.01$.

upon stimulation with TLR agonists, except agonists for TLRs 5 and 7 (Fig. 6 A). Interestingly, among all TLR ligands, treatment with LPS showed the greatest repression of *bdh2* expression (Fig. 6 A). This observation corroborates the finding that *bdh2*-null mice are resistant to LPS producing *E. coli*. In primary macrophages derived from mouse bone marrow treatment with LPS also repressed *bdh2* message (Fig. 6 B).

LPS target genes are either repressed or induced in a temporal cascade. Genes encoding proinflammatory cytokines are transiently induced with peak expression at ~4 h after LPS

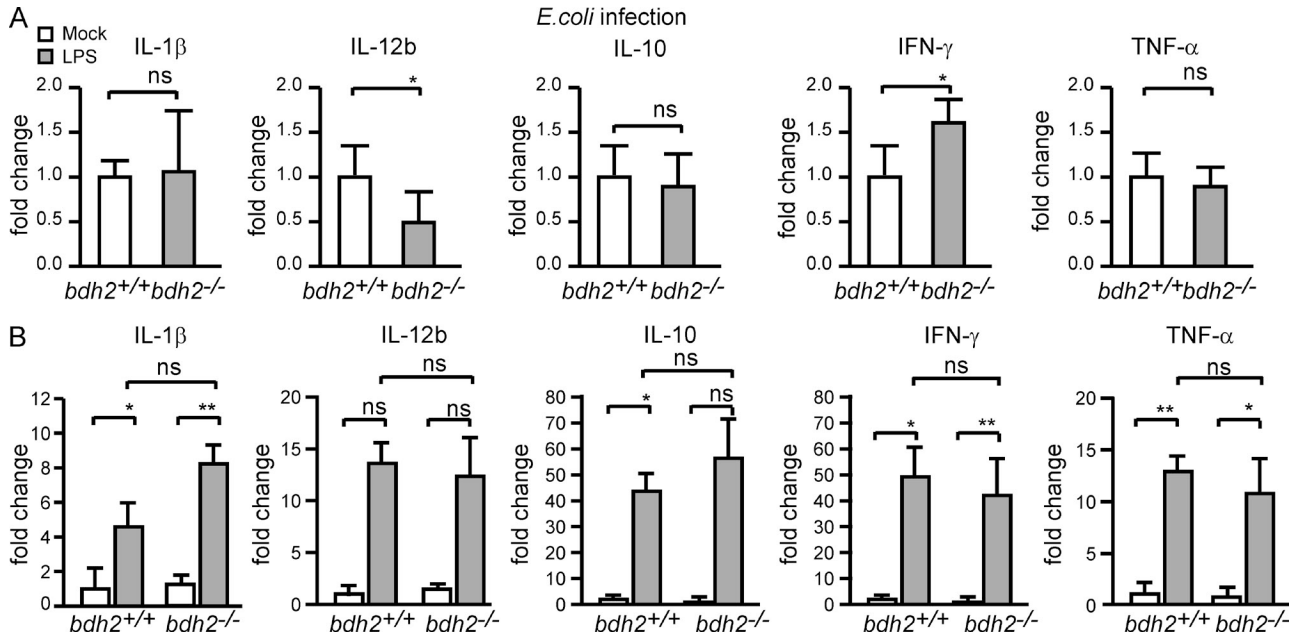

Figure 5. Analysis of cytokines in *bdh2*-null mice. (A) Quantification of mRNAs for indicated cytokines in liver samples of control or *bdh2*-null mice 36 h after infection with *E. coli* H9049. Expression levels of cytokine mRNAs as indicated with control mice set at 1. The relative mRNA levels in each sample were normalized to actin mRNA. Results show pooled data from two independent experiments, each with at least three mice per group. Statistical analysis by two-tailed unpaired Student's *t* test: ns, not significant; *, $P < 0.05$. (B) Quantitative analysis of mRNAs for indicated cytokines in liver samples of control or *bdh2*-null mice 6 h after LPS injection. Values relative to the liver mRNA from PBS-injected mice. Results show pooled data from two independent experiments, each with at least three mice per group. Statistical analysis by one-way analysis of variance followed by the Tukey HSD test for multiple comparisons: ns, not significant; *, $P < 0.05$; **, $P < 0.01$.

treatment (Aung et al., 2006). Therefore, the observed repression of *bdh2* may be secondary to autocrine effects of cytokines. To test this possibility, we performed a kinetic analysis of *bdh2* levels in macrophages stimulated with LPS. We first detected repression of *bdh2* 1 h after LPS treatment, which preceded detection of cytokines in the medium (Fig. 6 C). Addition of cycloheximide, a protein synthesis inhibitor, to LPS-treated macrophages resulted in a decrease in *bdh2* expression, but inhibited synthesis and secretion of IL-6, one of the major cytokines induced by LPS (Fig. 6 D; Akira et al., 1993). However, repression of *bdh2* in cycloheximide + LPS-treated cells is moderate compared with cells treated with LPS alone (Fig. 6 D). Because cycloheximide treatment inhibits global protein synthesis, this would include transcription factors that repress *bdh2* (see below). Finally, to directly test the regulatory role of cytokines on *bdh2* expression, we treated macrophages with recombinant cytokines and analyzed *bdh2* expression. We found that most cytokines had no effect on *bdh2* expression (Fig. 6 E). Collectively, these results suggest that *bdh2* is regulated directly by LPS.

To assess whether LPS stimulation down-regulates *bdh2* expression in vivo, WT mice were challenged with LPS and *bdh2* mRNA was quantitated by real-time PCR analysis. LPS stimulation significantly reduced *bdh2* mRNA in liver samples of WT mice (Fig. 6 F). Because LPS is a major component of the *E. coli* outer cell wall, we asked whether *bdh2* levels are altered by *E. coli* infection. There was a significant reduction of both *bdh2* mRNA and protein in *E. coli*–infected mice (Fig. 6, G and H). In contrast, 24p3 levels were significantly induced (Fig. 6 I). The 2,5-DHBA level in these mice paralleled *bdh2* levels (Fig. 6 J). Interestingly, *S. aureus* infection also repressed *bdh2* and lowered 2,5-DHBA levels, whereas 24p3 levels were higher (Fig. 6, G–J). 2,5-DHBA supplementation does not alter *S. aureus* growth and *bdh2*-null mice display phenotypic characteristics comparable to WT mice upon *S. aureus* challenge (Figs. 1 and 3). The significance of *bdh2* repression in *S. aureus*–challenged mice is currently unknown. Nonetheless, the higher levels of 24p3 may further boost host defense in *bdh2*-null mice, thus explaining, in part, the resistance of *bdh2*-null mice to *E. coli* infection.

LPS binds to TLR4 and initiates a signaling pathway culminating in initiation of inflammation (Lu et al., 2008). To determine whether LPS-induced repression of *bdh2* depends on TLR4, we analyzed *bdh2* expression in $TLR4^{-/-}$ mice. Basal levels of *bdh2* mRNA were similar in WT and $TLR4^{-/-}$ mice (Fig. 6 K). Significantly, LPS-dependent repression of *bdh2* mRNA was abolished in the liver and spleen of $TLR4^{-/-}$ mice (Fig. 6 K). These observations suggest that TLR signaling regulates *bdh2* expression.

The transcription factor BLIMP mediates LPS-induced repression of bdh2

We investigated the molecular basis by which TLR4 represses *bdh2* expression. Because TLR-mediated gene regulation occurs predominantly via transcriptional regulation, we examined

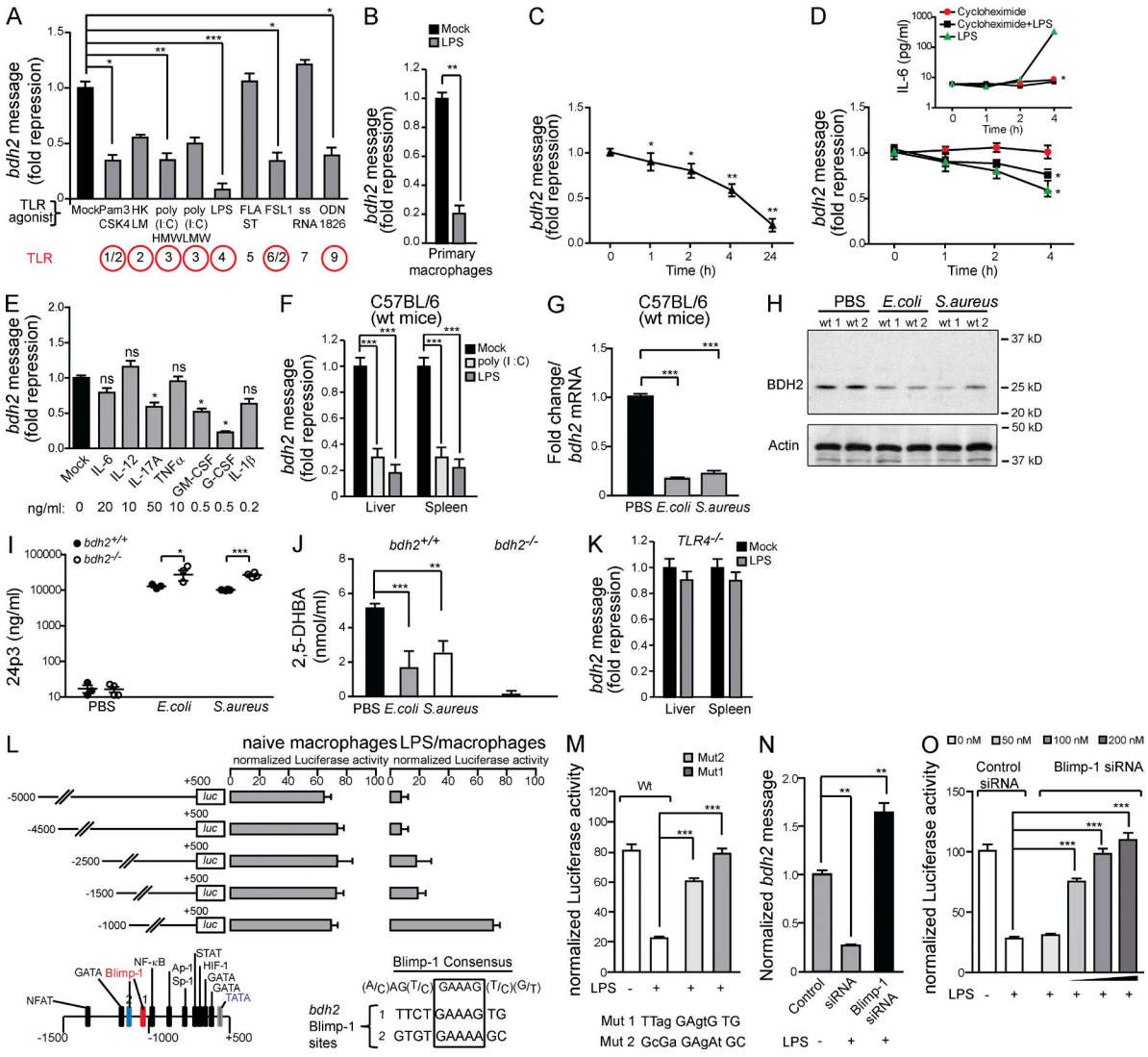

Figure 6. Bdh2 production is repressed by TLRs. (A) Quantitative analysis of *bdh2* mRNA 4 h after treatment of RAW264.7 macrophages with the indicated TLR ligands. Expression of levels of *bdh2* in naive cells was set at 1. The relative mRNA levels in each sample were normalized to *actin* mRNA. Data are the means of three independent experiments ± SD. Statistical analysis by one-way analysis of variance followed by the Tukey HSD test for multiple comparisons: *, $P < 0.05$, **, $P < 0.01$, ***, $P < 0.001$. (B) Quantitative analysis of *bdh2* mRNA 4 h after treatment of primary bone marrow macrophages with LPS. Analysis was as described in A. Results are the means of three independent experiments ± SD. Statistical analysis by two-tailed unpaired Student's *t* test: **, $P < 0.01$. (C) Time-course analysis of *bdh2* mRNA at the indicated time points after LPS treatment of RAW264.7 macrophages. The expression level of *bdh2* in naive cells was set at 1. Results are the means of three independent experiments ± SD. Statistical analysis by one-way analysis of variance followed by the Tukey HSD test: *, $P < 0.05$; **, $P < 0.01$. (D) Analysis of *bdh2* mRNA in LPS-treated RAW264.7 macrophages with or without cycloheximide. The expression level of *bdh2* in cycloheximide only treated cells was set at 1. Inset, IL-6 levels in culture supernatants from the same cells determined by ELISA. The results are the means of three independent experiments ± SD. Statistical analysis by one-way analysis of variance followed by the Tukey HSD test: *, $P < 0.05$. (E) Effect of cytokines on *bdh2* mRNA level in RAW264.7 macrophages. Cells were treated with the indicated amounts of recombinant cytokines for 12 h and *bdh2* mRNA levels were determined by qRT-PCR. The expression level of *bdh2* mRNA in untreated cells was set at 1. The results are the means of three independent experiments ± SD. Statistical analysis by one-way analysis of variance followed by the Tukey HSD test: ns, not significant; *, $P < 0.05$. (F) Quantitative analysis of *bdh2* mRNA in liver and spleen samples of 8-wk old female C57BL/6 WT mice after poly (I:C) or LPS injection. Values relative to the mRNA from PBS-injected mice. Analysis was as described in A. Results show pooled data from two independent experiments, each with at least three mice per group. Statistical analysis by one-way analysis of variance followed by the Tukey HSD test: ***, $P < 0.001$. (G) Quantitative analysis of *bdh2* mRNA in liver samples of 8-wk-old female C57BL/6 WT mice after *E. coli* or *S. aureus* infection. Values relative to the mRNA from PBS-injected mice. Analysis was as described in A. Results show pooled data from two independent experiments, each with at least three mice per group. Statistical analysis by one-way analysis of variance followed by the Tukey HSD test: ***, $P < 0.001$. (H) Immunoblot analysis of Bdh2 in C57BL/6 WT mice after *E. coli* or *S. aureus* infection. Actin was used as a loading control. Molecular weight markers are indicated on the right. (I) Quantitative analysis of 24p3 in serum samples of WT and *bdh2*-null mice after *E. coli* H9049 or *S. aureus* infection. Symbols represent individual mice. Bars represent the mean values. Data are representative of two independent experiments, each with at least three to four mice per group. Statistical analysis

the motifs in the promoter region of *bdh2* that confer TLR-dependent down-regulation. We initially analyzed transcriptional regulation of the *bdh2* gene in naive RAW264.7 macrophages. A 5′-RACE PCR identified the transcription start site ∼25 bp downstream of a TATA box (Fig. 6 L). We then cloned the 5′-flanking region spanning −5 kb to + 0.5 kb relative to the transcription start site into a firefly luciferase reporter plasmid. Constitutive reporter gene activity was detectable in RAW264.7 cells (Fig. 6 L). Consistent with endogenous *bdh2* mRNA expression, stimulation of RAW264.7 cells via the TLR4 pathway significantly reduced luciferase activity (Fig. 6 L). To identify the cis-acting DNA elements that confer TLR-dependent regulation on *bdh2*, we constructed progressive 5′ deletion mutants of the *bdh2* promoter and analyzed their activity (Fig. 6 L). All the mutants retained basal activity in naive macrophages (Fig. 6 L). However, TLR-mediated repression of luciferase activity was lost when a deletion from −1.5 kb to −1 kb bp was analyzed, indicating positive *cis*-acting regulatory elements in this region (Fig. 6 L).

A careful analysis of this region using Transcription Element Search Software identified two putative binding sites for Blimp-1 (B lymphocyte-induced maturation protein-1), a DNA-binding factor that is critical for the differentiation of myeloid cells. Blimp-1 is a transcriptional repressor that recruits histone deacetylases, histone lysine/arginine methyltransferases, and co-repressors to induce promoter silencing (John and Garrett-Sinha, 2009). The Blimp-1–binding motif closest to the transcription start site bears significant homology to the consensus sequence (Fig. 6 L). Significantly, Blimp-1 is induced by LPS and mediates silencing of dependent promoters in a TLR-dependent manner (Lord et al., 2009). Thus, Blimp-1 may suppress *bdh2* expression. To test this possibility, we mutated the two Blimp-1–binding sites in the mouse *bdh2* promoter. Stimulation with LPS failed to repress the *bdh2* promoter bearing mutations in both the Blimp-1–binding sites, indicating that Blimp-1–binding sites mediate LPS repression of the *bdh2* promoter (Fig. 6 M).

To rigorously test the role of Blimp-1 in LPS-mediated repression of *bdh2*, we suppressed endogenous Blimp-1 in LPS-treated RAW264.7 macrophages by RNAi-mediated silencing. Quantitative real-time PCR analysis suggested down-regulation of *blimp-1* in LPS-treated RAW264.7 cells (not depicted). We also confirmed these results by performing immunoblot analysis using an anti–Blimp-1 antibody. We first analyzed endogenous *bdh2* message in *blimp-1* silenced RAW264.7 cells that were stimulated with LPS. *Bdh2* mRNA levels were unaltered despite LPS treatment in *blimp-1* knock down cells (Fig. 6 N). Next, we transfected a *bdh2-luc* reporter into *blimp-1*–silenced, LPS-treated RAW264.7 cells. In agreement with the results of Fig. 6 N, Blimp-1 deficiency abrogates LPS-mediated repression of *bdh2* (Fig. 6 O). Together, these results confirm that Blimp-1 mediates LPS-induced repression of *bdh2*.

Hepcidin–ferroportin axis is deregulated in *E. coli*–infected bdh2-null mice

Serum iron levels are decreased during infection to starve the invading bacteria of iron (Ganz, 2009). Hypoferremia associated with infection is mediated by hepcidin (Ganz and Nemeth, 2012; Drakesmith and Prentice, 2012). Naive *bdh2*-null mice have lower serum iron when compared with WT mice (Fig. 7 A). However, upon injection of sublethal doses of *E. coli*, serum iron was even lower in *bdh2*-null mice compared with *E. coli*–injected WT mice (Fig. 7 A). The reduction in serum iron in the absence of 2,5-DHBA further restricts bacterial replication in *bdh2*-null mice.

Hepcidin binds to ferroportin on the plasma membrane of enterocytes, macrophages, hepatocytes, and other cells promoting its internalization and eventual lysosomal degradation (Nemeth et al., 2004; De Domenico et al., 2007). Hepcidin-independent mechanisms also regulate ferroportin (Deschemin and Vaulont, 2013). Inactivation of ferroportin by hepcidin leads to intracellular iron retention (Nemeth et al., 2004). We therefore assessed the levels of hepcidin and ferroportin in liver and spleen samples, respectively, from uninfected as well

by two-tailed unpaired *t* test: *, P < 0.05; ***, P < 0.001. (J) Assessment of 2,5-DHBA levels in urine samples of control and *bdh2*-null mice challenged with *E. coli* H9049 or *S. aureus*. Mass spectrometry analysis of cold ethanol precipitated urine samples. 2,5-DHBA levels were quantitated by comparing to known amounts of 2,5-DHBA. Results show pooled data from two independent experiments, each with at least three mice per group. Statistical analysis by one-way analysis of variance followed by the Tukey HSD test: **, P < 0.01; ***, P < 0.001. (K) Quantitative analysis of *bdh2* mRNA in liver and spleen samples of LPS-injected *TLR4*-null mice. Values relative to the mRNA from PBS-injected mice. Analysis was as described in A. Results show pooled data from two independent experiments, each with at least three mice per group. Statistical analysis by two-tailed unpaired Student's *t* test: P < 0.05 was considered significant. (L) The *bdh2* promoter is down-regulated by LPS stimulation in RAW264.7 macrophages. Progressive deletions in 5′ flanking region of the *bdh2* gene. (left) Luciferase activity in naive RAW264.7 cells. (right) Luciferase activity in LPS-stimulated RAW264.7 cells. Bottom, predicted transcription factor binding sites. The DNA binding site for Blimp-1 is shown. Results are means of three independent experiments ± SD. (M) Mutations in Blimp-1 binding sites in murine *bdh2* promoter blunts LPS-mediated repression. Base substitutions are indicated below. RAW264.7 cells were transfected with WT (−1.5 to +0.5 kb) or mutant bdh2-*luc* reporter plasmids containing base substitutions and luciferase activity was determined as in G. Results are the means of three independent experiments ± SD. Statistical analysis by one-way analysis of variance followed by the Tukey HSD test: ***, P < 0.001. (N) Blimp-1 silencing abrogates TLR4-mediated repression of *bdh2* in RAW264.7 macrophages. *Bdh2* message was quantified in LPS treated and Blimp-1 deficient RAW264.7 cells. The relative mRNA levels in each sample were normalized to *actin* mRNA. Results are the means of three independent experiments ± SD. Statistical analysis by one-way analysis of variance followed by the Tukey HSD test: **, P < 0.01. (O) Luciferase activity in Blimp-1 repressed cells. RAW264.7 cells were co-transfected with the *bdh2-luc* reporter (−1.5 to +0.5 kb) and with either increasing amounts of *blimp-1* siRNA or control siRNA and the luciferase activity was determined after LPS stimulation as in G. Results are the means of three independent experiments ± SD. Statistical analysis by one-way analysis of variance followed by the Tukey HSD test: ***, P < 0.001.

as *E. coli*–infected WT and *bdh2*-null mice. Hepcidin levels were the same in uninfected WT and *bdh2*-null mice (Fig. 7 B). Infection with *E. coli* transiently increased hepcidin levels in both WT and *bdh2*-null mice (Fig. 7 B). However, hepcidin levels in *E. coli*–infected *bdh2*-null mice were significantly higher than in infected WT mice at 3 h after infection (Fig. 7 B). Hepcidin levels in both groups of mice decreased by 6 h after infection, perhaps in response to lower serum iron (Fig. 7, A and B).

We next assessed ferroportin levels in uninfected and *E. coli*–infected mice from both genotypes. Upon infection with *E. coli*, ferroportin levels in WT mice were decreased at both time points after infection (Fig. 7 C). However, in *E. coli*–infected *bdh2*-null mice, ferroportin levels were significantly decreased compared with infected WT mice at both time points (Fig. 7 C). Collectively, the results of Figs. 7 (B and C) suggest that ferroportin levels are decreased in *E. coli*–infected *bdh2*-null mice.

DISCUSSION

To prevent bacterial iron acquisition, mammals deploy an elaborate set of mechanisms to withhold iron. One of these mechanisms involves TLR regulation of lipocalin 24p3, a chelator of bacterial siderophores (Flo et al., 2004). 24p3 is a unique iron-binding protein in that it lacks the ability to bind iron directly. Iron binding by 24p3 is mediated by a small molecule, e.g., a siderophore (Goetz et al., 2002). By sequestering iron-laden bacterial siderophores, 24p3 functions as a bacteriostat. As predicted, *24p3*-null mice are hypersensitive to bacterial septicemia (Flo et al., 2004; Berger et al., 2006). However, this line of host defense is limited by 24p3′s ability to only sequester a subset of bacterial siderophores (Holmes et al., 2005). Additionally, pathogenic bacteria secrete multiple siderophores or chemically modify them to prevent capture by 24p3 (Fischbach et al., 2006; Henderson et al., 2009).

Members of the SDR family of dehydrogenases are implicated in disparate cellular processes (Oppermann et al., 2003). Based on a computational design, Bdh2, or DHRS6, was proposed to bind and oxidize ketone bodies in the cytoplasm (Guo et al., 2006). Several lines of evidence suggest that Bdh2 may be dispensable for oxidation of ketone bodies: 1) Bdh2 deficiency does not alter ketone body levels; 2) cytosolic Bdh2 is only 20% identical to Bdh1, a mitochondrial enzyme involved in NAD^+/NADPH-dependent oxidation/reduction of ketone bodies (Guo et al., 2006; Cotter et al., 2013); 3) a majority of ketone bodies are ferried into mitochondria to fuel energy reactions. Therefore the contribution of Bdh2 to cytosolic ketone oxidation seems to be minimal.

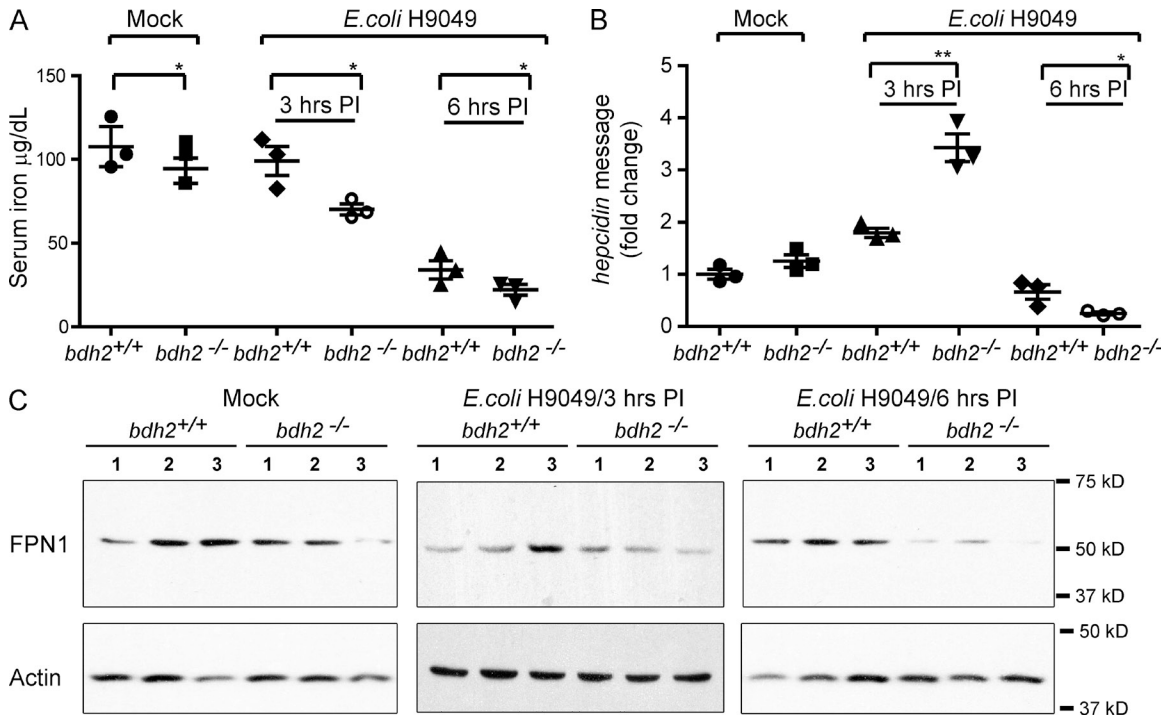

Figure 7. Analysis of iron parameters in *E. coli* H9049–infected WT and *bdh2*-null mice. (A) Serum iron in naive and *E. coli* H9049–infected C57BL/6 WT and *bdh2*-null mice. Mice were infected with 6×10^7 CFU of *E. coli* H9049 and serum iron was determined 3 and 6 h after infection. Data are representative of two independent experiments, each with at least three mice per group. Statistical analysis by two-tailed unpaired Student's *t* test: *, $P < 0.05$. (B) Quantification of *hepcidin* mRNA in WT or *bdh2*-null mice 3 or 6 h after infection with 6×10^7 CFU of *E. coli* H9049. Expression levels of hepcidin mRNA in control mice was set at 1. The relative mRNA levels in each mouse were normalized to actin mRNA. Data are representative of two independent experiments, each with at least three mice per group. Statistical analysis by two-tailed unpaired Student's *t* test: *, $P < 0.05$; **, $P < 0.01$. (C) Immunoblot analysis of ferroportin in spleen samples from WT or *bdh2*-null mice infected with 6×10^7 CFU of *E. coli* H9049. Actin was used as a loading control. Spleen samples from three mice were used. Molecular weight markers are indicated on the right.

Previously we showed that Bdh2 catalyzes 2,5-DHBA synthesis (Devireddy et al., 2010). Our current results confirm that cytosolic Bdh2 is important for 2,5-DHBA synthesis and that Bdh2 is not involved in ketone body metabolism: first, mammalian Bdh2 is highly homologous to bacterial EntA (>45% similarity and ~31% identical; Devireddy et al., 2010), which oxidizes 2,3-dihydro 2,3-DHBA to 2,3-DHBA. The high degree of homology suggests that the major function of Bdh2 is DHBA synthesis; second, in agreement with the above prediction, we showed that the absence of Bdh2 abrogates 2,5-DHBA biosynthesis both in vivo and in cultured cells (Devireddy et al., 2010; this study); third, contrary to the purported function based on a computational study (Guo et al., 2006), ketone body levels are unchanged in *bdh2*-null mice; finally, the absence of *bdh2* results in alterations in cellular iron metabolism both in vivo and in cell culture models (Devireddy et al., 2010). All of these results strongly support a role for Bdh2 in the synthesis of 2,5-DHBA in mice.

Recent studies demonstrated that 24p3 binds to endogenous 2,5-DHBA or catechol (Yang et al., 2003; Bao et al., 2010; Devireddy et al., 2010). As noted by Jones et al. (1980), very little is known about the small molecular weight iron binding molecules in mammalian tissues or their interaction with bacteria. Further, the role of these compounds in 24p3-mediated host defense remains elusive. This report supports the hypothesis that mammalian siderophore-like molecules augment bacterial growth by facilitating iron import into bacteria. Bacteria secrete a variety of siderophores to acquire iron from the host. However, the secreted siderophores are hijacked by a variety of host-derived proteins, e.g., 24p3. In this regard, 2,5-DHBA, which is ubiquitous, may serve as an alternative source for invading pathogens to obtain iron. To counter the hijacking of 2,5-DHBA, the host suppresses *bdh2* expression thus depriving the bacteria the added opportunity presented by 2,5-DHBA. Additionally, serum iron levels are lower in *bdh2*-null mice (unpublished data). The combined effects of lower serum iron and the absence of 2,5-DHBA provide an effective response by the host. Unlike 2,5-DHBA, catechol adversely affects growth of bacteria via an unknown mechanism (Park et al., 2001); the function of the catechol–24p3 complex in host defense is unclear.

Cytokines, the major effectors of infection, were unaltered in *bdh2*-null mice. We found that IFN-γ was differentially regulated in macrophages of *bdh2*-null mice upon challenge with *E. coli,* but not with LPS. Although the major antigenic determinant of *E. coli* is LPS, we did not observe altered IFN-γ in response to LPS challenge. The basis for this discrepancy is unclear, but it is possible that active replication of *E. coli* may be necessary to alter IFN-γ in *bdh2*-null mice. High levels of IFN-γ alter intracellular iron homeostasis in macrophages and promote intracellular defenses against invading pathogens (Gordon et al., 2005). Therefore, higher levels of IFN-γ in *bdh2*-null mice may in part explain the decrease in *M. tuberculosis* replication in *bdh2*-null mice.

In contrast to most innate immune genes, *bdh2* expression is down-regulated after activation of macrophages with TLR agonists, more so with TLR4 ligand. Negative regulators of TLR signaling are often induced after activation. For instance, IRAK-M, an inhibitor of IRAK-1 signaling, is induced by LPS treatment to promote tolerance to future LPS challenges (van 't Veer et al., 2007). Blimp-1 is another LPS-induced transcription factor that down-regulates downstream targets, perhaps to induce a full inflammatory response (John and Garrett-Sinha, 2009). So, what is the significance of *bdh2* down-regulation by Blimp-1? Based on our findings, we hypothesize that *bdh2* is present before immune stimulation, but that during infection its expression is reduced to prevent bacterial utilization of 2,5-DHBA for iron scavenging. We provided further mechanistic detail by showing that Blimp-1 is the major factor that confers LPS-mediated transcriptional repression of *bdh2*. Other factors may also play a role in the LPS-mediated down-regulation of *bdh2*. For example, LPS treatment differentially affects a set of miRNAs whose function is to change inflammatory status (Tili et al., 2007). Finally, down-regulation of *bdh2* in *S. aureus*–infected mice suggests additional regulatory mechanisms that remain to be elucidated.

We found that serum iron levels are low in *bdh2*-null mice. How *bdh2* deficiency contributes to lower serum iron is unclear. However, we believe that iron export from the spleen is faulty in *bdh2*-null mice. Several lines of evidence support this hypothesis: (1) we found that *bdh2*-null mice accumulate iron in the spleen and to a limited extent in liver (unpublished data); and (2) macrophages recycle heme from senescent RBC and store iron in ferritin, which is directed to the lysosomal pathway to meet cellular demands for iron. Ferroportin regulates iron egress from macrophages into the circulation (Delaby et al., 2005). Free heme is very toxic, and lack of the antioxidant 2,5-DHBA (Joshi et al., 2012) leads to a nonenzymatic destruction of heme, removing iron from its normal path toward ferroportin. The scenario of high iron in liver/spleen and low serum iron in *bdh2*-null mice is reminiscent of anemia of chronic disease.

The mammalian siderophore and 24p3 are reciprocally regulated by TLR4 (Flo et al., 2004). This raises the possibility that the mammalian siderophore and 24p3 cooperatively protect mice from infection. The reciprocal regulation of *24p3* and *bdh2* by TLR4 agonist serves two purposes: (1) down-regulation of the mammalian siderophore allows 24p3 to bind only the siderophores secreted by invading pathogens because 24p3 binds both mammalian and bacterial siderophores (Holmes et al., 2005; Devireddy et al., 2010), thus maximizing the sequestering activity of 24p3; and (2) because 2,5-DHBA augments *E. coli* growth, suppression of 2,5-DHBA by TLR signaling deprives the bacteria of the added growth advantage conferred by 2,5-DHBA. This observation helps to explain an earlier study that demonstrated the ability of mammalian cell extracts to potentiate bacterial growth (Jones et al., 1980).

MATERIALS AND METHODS

Cells and reagents. RAW264.7 cells were cultured in Dulbecco's modified Eagle's medium supplemented with 10% fetal bovine serum, 2 mM L-glutamine, 100 U of Penicillin, and 100 µg Streptomycin (Invitrogen). LPS

derived from *E. coli* 011:B5 was purchased from Sigma-Aldrich and used at 100 ng/ml. A set of TLR ligands was obtained from InvivoGen. All DHBAs were purchased from Sigma-Aldrich. Stock solutions of DHBAs were made in aqueous NaOH. Anti-Bdh2 antibody was purchased from Santa Cruz Biotechnology, Inc. Anti-actin antibody was purchased from Sigma-Aldrich. Anti-ferroportin antibody was purchased from OriGene. Recombinant cytokines were purchased from PeproTech. Oligonucleotides were purchased from Invitrogen.

Targeted mutagenesis of murine bdh2. Catalytic activity of Bdh2 is dependent on NPG and SYK motifs, which are encoded by *exon* 7 (Guo et al., 2006). Mutations in this region blunt the enzymatic activity of Bdh2 and abrogate the biogenesis of 2,5-DHBA (Devireddy et al., 2010). Additionally, amino acid residues encoded by *exon* 7 of *bdh2* form a helix, which is located at a dimer interface within the tetramer (Guo et al., 2006). So removal of this stretch of helices prevents proper dimer/tetramer formation and within this helical stretch of residues are 3 aa, which form the active site: Tyr147 and Lys151 interact with the bound NAD^+ cofactor and Arg144 interacts with a sulfate in the active site (Guo et al., 2006). Thus, removal of amino acids, which are coded by *exon* 7, results in abrogation of the enzymatic activity of Bdh2 and also destabilizes the structure of Bdh2. Therefore, we replaced *exon* 7 of *bdh2* gene with a *neomycin* resistance cassette.

The targeting strategy modified a 10-kb region containing the *exon* 7 of the murine *bdh2* genomic locus (Fig. 2 A). The 129S7/SvEv BAC clone (BMQ-320-G12) covering the region of murine *mbdh2* was obtained from Source BioScience. For targeting construct preparation, we used MCI-TK vector (from G. Luo, Case Western Reserve University, Cleveland, OH). *Lox P*-flanked linker was inserted into Asp718 site in *intron* 7 and a third *Lox P* site was inserted into XhoI site in *intron* 8 (Fig. 2 A). Coding sequence for *thymidine kinase* was present outside of the homology regions. The targeting construct was electroporated into Cre expressing (Cre recombinase under the control of *Protamine 1* promoter; O'Gorman et al., 1997) R1 ES cells (129 background) and transfected cells were selected for resistance to G418 (Invitrogen) and ganciclovir (EMD Millipore).

Two homologously recombined clones with a normal karyotype were injected into C57BL/6 mouse blastocysts, and then were transferred into the uteri of pseudopregnant females. Highly chimeric male (>90%) were bred with C57BL/6 females to generate F1 offspring carrying the modified *bdh2* allele. Germline transmission of the modified *bdh2* allele was determined by Southern blot analysis of tail DNA samples. ES cells used for gene targeting in this study express Cre recombinase in male germ cells resulting in germline deletion of floxed *exon* 7 (O'Gorman et al., 1997). Conversion to null mutation was confirmed by Southern blotting or PCR using primers listed in Table 1. Subsequent genotyping was performed by PCR analysis of DNA from tail snips. We then backcrossed *bdh2*-null mice onto C57BL/6 or 129 SvimJ genetic background successively for at least nine generations.

Bdh2-null and wild-type littermates were obtained by intercrosses of *bdh2* heterozygous mice. To assess the specificity of the *bdh2*-targeted deletion, we confirmed the deletion of *exon* 7 by either genomic DNA PCR or RT-PCR in bone marrow cells or in kidney. *Bdh2*-null mice on C57BL/6 genetic background were analyzed in this report.

Southern blot and PCR genotyping. For Southern blot analysis, 20 µg of genomic DNA was digested overnight with Asp718, fractionated on a 0.5% agarose gel, and transferred onto Hybond N+ membrane (GE Biosciences). The probe for Southern blots was derived by PCR amplification of a region encompassing *exon* 7 using primers 5′-TCACTCACTCTTCAAAGGGAAAGCTG-3′ and 5′-CTCGAGTGTCCTGGAACTCACTCTGTAGACC-3′. The amplified PCR product was labeled by random priming in the presence of [^{32}P]dCTP using a kit from Stratagene as per the manufacturer's instructions. The probe was then hybridized to genomic DNA cross-linked to Nylon membrane. Hybridized DNA was visualized by autoradiography.

We routinely genotyped mice by PCR analysis using primers whose sequences are listed in Table 1. Genomic DNA from tail snips was isolated using a kit from QIAGEN. DNA was then subjected to PCR analysis using a cocktail of PCR primers. Amplified fragments were visualized in ethidium bromide stained agarose gels.

Bacterial strains and determination of bacterial growth. WT and mutant strains bearing mutations or deletions in *aroB* or *fepA* or *aroB* and *fep*A (a gift from by K. Postle, Penn State University, University Park, PA) were cultivated in LB for initial propagation. To study the effect of various isoforms of DHBA, we cultured bacteria in RPMI supplemented with graded doses of DHBA solubilized in water. After overnight incubation, CFU were determined by plating on LB agar plates. To study the effect of iron and DHBA supplementation on bacterial growth, graded doses of $FeCl_3$ was added to a fixed dose of DHBA and CFU were determined as described above.

Animals. All animal protocols were approved by the Institutional Animal Care and Use committee of Case Western Reserve University. Animals were maintained on standard laboratory diet. *Bdh2*-null mice were maintained on either C57BL/6 or 129 SvimJ genetic background. Age- and sex-matched adult mice on comparable genetic background were used for experiments. Mice were housed in microisolator cages and received food and water ad libitum. *TLR4*-null mice were a gift from A. Hise (Center for Global Health and Diseases, Case Western Reserve University, Cleveland, OH). All experimental protocols were performed in accordance with IACUC guidelines and were approved by the institutional animal resources center.

Table 1. Sequences for primers

PCR primers	Sequence (5′ to 3′)	Notes
P1	ACCAGACTCGGCTTCAGAGTCTGTG	Forward
P2	TCTTGTCTGAGTTGTAACCTCAAGG	Reverse
P3	GGCAGGCGGATCTCTGAGTTCAAGG	Forward
P4	CTCGCTCTCTTGCGCTCTCGTCTTG	Reverse
Hamp	AGCAGCACCACCTATCTCCATCAA	Forward
Hamp	TGCATTGGTATCGCAATGTCTGCC	Reverse
Bdh2	GATGCAACTGTGTGTGTCCAGGAA	Forward
Bdh2	ACAGGGTTGCCAGTTACATAGGCT	Reverse
Actin	TGTTACCAACTGGGACGACA	Forward
Actin	GGGGTGTTGAAGGTCTCAAA	Reverse

Gas chromatography-mass spectrometry. To assess 2,5-DHBA levels in WT and *bdh2*-null mice, urine samples were mixed with cold absolute ethanol. Precipitated material was removed by centrifugation. The supernatant was then vacuum dried and derivatized with BSTFA-pyridine (*N,O-bis*[Trimethylsilyl]trifluoroacetamide; Thermo Fisher Scientific) 1:1 at 80°C for 1 h, and then subjected to GC-MS. The NIST library search was performed against 191,436 MS spectra. DHBA standards were obtained from Sigma-Aldrich.

Derivation of ^{13}C labeled 2,5-DHBA. The ^{13}C-carboxy-salicylic acid (Fluka) was solubilized in 0.23 N KOH to yield a 0.4-mM solution. This solution was chilled to 0°C on an ice bath and aqueous solution of $K_2S_2O_8$ (0.48 mM) was slowly added over a period of 1 h. The reaction mixture was then allowed to return to room temperature and stirred for 18 h at room temperature. Later, 1.5 ml of concentrated H_2SO_4 was added to the reaction mixture and boiled for 45 min. The reaction mixture was then cooled and subjected to ethyl acetate extraction. The combined organic layer was then dried over anhydrous Na_2SO_4. The end product was purified on a silica gel column using MeOH–CH_2Cl_2 (1:9). The eluted material contained the ^{13}C-carboxy-2,5-DHBA. This procedure routinely yielded ^{13}C-2,5 DHBA at 40%. Purity of the derived ^{13}C-2,5 DHBA was confirmed by 400 MHz ^{1}HNMR and 100 MHz ^{13}CNMR.

Metabolite measurements in plasma. Plasma samples from WT and *bdh2*-null mice were analyzed for 3-hydroxybutyric acid and acetoacetate using a kit from Wako diagnostics as per manufacturer's instructions. Plasma triglycerides, cholesterol, and free fatty acids were analyzed by Marshfield Laboratories.

Plasmids and molecular cloning strategy. For TLR regulation studies of *bdh2* promoter, a Luciferase reporter containing the *bdh2* upstream regulatory region was cloned as indicated below. A PCR generated ~5-kb fragment containing *bdh2* promoter was inserted upstream of the *luciferase* gene (*luc2*) in pGL4.13 vector (Promega) to generate the *bdh2*-Luc WT promoter vector. We also derived several deletion constructs within the promoter region of *bdh2* promoter by linker scanning mutagenesis. Site-directed mutagenesis was performed to modify Blimp-1–binding sites in *bdh2* promoter using a QuikChange site-directed mutagenesis kit from Stratagene. All reporter plasmids were sequence verified.

Luciferase assays. RAW 264.7 cells at 50–60% confluency cultured in a 6-well plate were transiently transfected with the indicated *bdh2-luc* reporter plasmids along with a control Renilla Luciferase plasmid (pGL4.74) using Lipofectamine transfection reagent from Invitrogen. An empty vector (pGL4.13) served as a negative control. After the removal of DNA complexes, cells were replated in a 24-well plate and treated for 16 h with LPS (Sigma-Aldrich). Firefly and Renilla luciferase activities of lysates were assayed using a Dual Luciferase Assay kit from Promega. All Luciferase measurements were normalized to the Renilla Luciferase expression to correct for differences in transfection efficiency.

Immunoblot analysis. Liver samples from WT and *bdh2*-null mice challenged with *E. coli* or *S. aureus* were resolved in discontinuous SDS-PAGE gels, transferred onto a Nitrocellulose membrane (Bio-Rad Laboratories) and probed with anti-BDH2 polyclonal antibody (Santa Cruz Biotechnology, Inc.). Blots were stripped and reprobed with anti-actin antibody (Sigma-Aldrich) to verify equal loading. Spleen samples from *bdh2*-null mice challenged with 6×10^7 CFU of *E. coli* were also resolved in discontinuous SDS-PAGE gels, transferred onto a Nitrocellulose membrane (Bio-Rad Laboratories), and probed with anti-ferroportin antibody (OriGene). Blots were stripped and reprobed with anti-actin antibody (Sigma-Aldrich) to verify equal loading.

ELISA. Serum samples were subjected to ELISA to measure 24p3 levels in WT and *bdh2*-null mice upon infection with *E. coli* or *S. aureus* using a kit purchased from R&D Systems as per the manufacturer's suggested procedure. IL-6 levels in culture supernatant from RAW cells supplemented with LPS were measured using a kit obtained from RayBiotech as per the manufacturer's instructions.

Serum and iron measurements. Whole blood was collected by terminal bleeding. Non-hemolyzed serum was collected and analyzed for total iron and transferrin saturation using a serum iron/TIBC (total iron-binding capacity) kit from Sigma-Aldrich as per manufacturer's instructions.

RNA interference. Control and *blimp-1* siRNAs were purchased from OriGene. Naive or LPS-stimulated RAW264.7 cells were transfected using Oligofectamine (QIAGEN). Knockdown efficiency was assessed by RT-PCR.

RNA isolation and gene expression analysis. Total RNA was isolated from naive or treated cells using TRIzol method (Invitrogen). DNase I (Promega) treated RNA was then reverse transcribed using Superscript III RT from Invitrogen as per manufacturer's recommendations. The resulting cDNAs were subjected to real time PCR analysis using SYBR Green master mix (Promega) following the manufacturer's recommendations. The fold-change was calculated using ΔΔCT method. qPCR results were normalized to either actin or 18S rRNA.

Experimental infection with *E. coli*, *S. aureus*, *C. albicans*, and *M. tuberculosis*. *E. coli* strains were propagated in LB and stock cultures were frozen in 15% glycerol containing growth medium. For inoculation experiments, bacteria were grown to midexponential phase ($OD_{600} = 0.5 - 0.7$). Bacteria were collected by centrifugation, washed twice with sterile PBS, and resuspended to 10^8 CFU/100 µl. Mice were inoculated intraperitoneally with indicated CFU. All the injected doses were verified by determining the CFU. Mice were examined for signs of disease at regular intervals and the mortality was recorded. All mice were sacrificed 7 d after inoculation.

For determination of bacterial loads, mice were infected with 0.6×10^8 CFU of *E. coli* H9049 (gift from Dr. Kelly Smith, University of Washington, Seattle, WA) and sacrificed 36 h after infection. Bacterial loads in blood, liver, and spleen were determined by plating serial dilutions of homogenates on to LB agar plates. Bacteria colonies were enumerated after incubation for 24 h at 37°C.

S. aureus (strain ATCC 25923) was cultured in trypticase soy broth (TSB), washed three times with PBS, and then resuspended in PBS for animal injection. Age- and sex-matched mice from each genotype were intraperitoneally injected with 1 ml PBS containing 3×10^8 *S. aureus*. The mortality in infected mice was recorded and plotted in Kaplan-Meier analysis.

Stock cultures of *C. albicans* (ATCC 562) were cultured in YM broth (BD). For experimental inoculation, cultures were propagated overnight in YM broth at 37°C and the blastoconidia were collected by centrifugation, washed with sterile PBS, and suspended in sterile PBS. The number of fungi was determined with a hemocytometer and their viability was determined by plating the diluted samples on YM agar plates. Mice (10 mice per group) were injected intraperitoneally with 7×10^7 cells of *C. albicans*. All the injected doses were verified by determining the CFU. The mortality in infected mice was recorded and plotted in Kaplan-Meier analysis.

M. tuberculosis (strain H37Rv) was propagated to mid-log phase on 7H10 agar plates. Colonies were then transferred to liquid GAS Media and grown to an absorbance of 1.1 (595 nm). The media was supplemented with 20% glycerol, allowed to settle for 5 min, and 3 ml aliquots were frozen at −80°C until use. Stock bacterial counts were determined by the CFU method. H37Rv infection stocks were prepared by diluting 1–1.5 ml of frozen bacterial stocks with sterile LPS-free water (Sigma-Aldrich). Bacterial clumps were disrupted by three sequential aspirations through a sterile 26-gauge hypodermic needle, and the 5-ml suspension placed in the glass nebulizer chamber of an Inhalation Exposure System (Glas Col) in the animal BSL-3 facility. Age- and gender-matched mice were aerosolized for 30 min as described (Anis et al., 2007). The initial *M. tuberculosis* inoculum was determined 1 d after infection and ranged between 100–200 CFU/lung homogenate. The mortality in infected mice was recorded and plotted in Kaplan-Meier analysis.

To determine *M. tuberculosis* loads at indicated points after infection, mice were sacrificed and their lungs were aseptically removed, weighed, and homogenized in saline. Homogenates were plated in duplicate onto 7H10 agar plates in 10-fold serial dilutions. Plates were incubated at 37°C and CFU were enumerated 14–18 d later.

Statistical analysis. Statistical analysis was performed using JMP statistical software. Data are represented as mean ± SD. Two-tailed Student's *t* test was applied for comparisons of two groups and Welch's correction was applied for unequal variance. One-way analysis of variance followed by the Tukey HSD (honestly significant difference) was applied for multiple comparisons. Survival was evaluated by the Kaplan-Meier log-rank test. For all tests, $P < 0.05$ was considered significant.

We thank Alan Tartakoff for editorial assistance; Kotty Postle for many helpful discussions; and Steve Macha for expert help in analyzing DHBA in mouse urine specimens.

This work is supported by R01DK081395, American Cancer Society Research Scholar Award, and Case Western Reserve University startup funds to L. Devireddy L. Devireddy is also a recipient of career developmental awards from March of Dimes and American Society of Hematology.

The authors declare no competing financial interest.

Submitted: 18 December 2013
Accepted: 25 April 2014

REFERENCES

Akira, S., T. Taga, and T. Kishimoto. 1993. Interleukin-6 in biology and medicine. *Adv. Immunol.* 54:1–78. http://dx.doi.org/10.1016/S0065-2776(08)60532-5

Albrecht-Gary, A.M., and A.L. Crumbliss. 1998. Coordination chemistry of siderophores: thermodynamics and kinetics of iron chelation and release. *Met. Ions Biol. Syst.* 35:239–327.

Almeida, R.S., D. Wilson, and B. Hube. 2009. *Candida albicans* iron acquisition within the host. *FEM. Yeast Res.* 9:1000–1012. http://dx.doi.org/10.1111/j.1567-1364.2009.00570.x

Anis, M.M., S.A. Fulton, S.M. Reba, C.V. Harding, and W.H. Boom. 2007. Modulation of naive CD4+ T-cell responses to an airway antigen during pulmonary mycobacterial infection. *Infect. Immun.* 75:2260–2268. http://dx.doi.org/10.1128/IAI.01709-06

Aung, H.T., K. Schroder, S.R. Himes, K. Brion, W. van Zuylen, A. Trieu, H. Suzuki, Y. Hayashizaki, D.A. Hume, M.J. Sweet, and T. Ravasi. 2006. LPS regulates proinflammatory gene expression in macrophages by altering histone deacetylase expression. *FASEB J.* 20:1315–1327. http://dx.doi.org/10.1096/fj.05-5360com

Bao, G., M. Clifton, T.M. Hoette, K. Mori, S.-X. Deng, A. Qiu, M. Viltard, D. Williams, N. Paragas, T. Leete, et al. 2010. Iron traffics in circulation bound to a siderocalin (Ngal)-catechol complex. *Nat. Chem. Biol.* 6:602–609. http://dx.doi.org/10.1038/nchembio.402

Barnard, T.J., M.E. Watson Jr., and M.A. McIntosh. 2001. Mutations in the *Escherichia coli* receptor FepA reveal residues involved in ligand binding and transport. *Mol. Microbiol.* 41:527–536. http://dx.doi.org/10.1046/j.1365-2958.2001.02473.x

Bentley, R. 1990. The shikimate pathway—a metabolic tree with many branches. *Crit. Rev. Biochem. Mol. Biol.* 25:307–384. http://dx.doi.org/10.3109/10409239009090615

Berger, T., A. Togawa, G.S. Duncan, A.J. Elia, A. You-Ten, A. Wakeham, H.E. Fong, C.C. Cheung, and T.W. Mak. 2006. Lipocalin 2-deficient mice exhibit increased sensitivity to *Escherichia coli* infection but not to ischemia-reperfusion injury. *Proc. Natl. Acad. Sci. USA.* 103:1834–1839. http://dx.doi.org/10.1073/pnas.0510847103

Beutler, B.A. 2009. TLRs and innate immunity. *Blood.* 113:1399–1407. http://dx.doi.org/10.1182/blood-2008-07-019307

Bleuel, C., C. Grosse, N. Taudte, J. Scherer, D. Wesenberg, G.J. Krauss, D.H. Nies, and G. Grass. 2005. TolC is involved in enterobactin efflux across the outer membrane of Escherichia coli. *J. Bacteriol.* 187:6701–6707. http://dx.doi.org/10.1128/JB.187.19.6701-6707.2005

Borregaard, N., and J.B. Cowland. 2006. Neutrophil gelatinase-associated lipocalin, a siderophore-binding eukaryotic protein. *Biometals.* 19:211–215. http://dx.doi.org/10.1007/s10534-005-3251-7

Braun, V., K. Günthner, K. Hantke, and L. Zimmermann. 1983. Intracellular activation of albomycin in *Escherichia coli* and *Salmonella typhimurium*. *J. Bacteriol.* 156:308–315.

Cassat, J.E., and E.P. Skaar. 2013. Iron in infection and immunity. *Cell Host Microbe.* 13:509–519. http://dx.doi.org/10.1016/j.chom.2013.04.010

Chaudhuri, S., J.M. Lambert, L.A. McColl, and J.R. Coggins. 1986. Purification and characterization of 3-dehydroquinase from Escherichia coli. *Biochem. J.* 239:699–704.

Cotter, D.G., R.C. Schugar, and P.A. Crawford. 2013. Ketone body metabolism and cardiovascular disease. *Am. J. Physiol. Heart Circ. Physiol.* 304:H1060–H1076. http://dx.doi.org/10.1152/ajpheart.00646.2012

De Domenico, I., D.M. Ward, C. Langelier, M.B. Vaughn, E. Nemeth, W.I. Sundquist, T. Ganz, G. Musci, and J. Kaplan. 2007. The molecular mechanism of hepcidin-mediated ferroportin down-regulation. *Mol. Biol. Cell.* 18:2569–2578. http://dx.doi.org/10.1091/mbc.E07-01-0060

Delaby, C., N. Pilard, A.S. Gonçalves, C. Beaumont, and F. Canonne-Hergaux. 2005. Presence of the iron exporter ferroportin at the plasma membrane of macrophages is enhanced by iron loading and down-regulated by hepcidin. *Blood.* 106:3979–3984. http://dx.doi.org/10.1182/blood-2005-06-2398

Deschemin, J.-C., and S. Vaulont. 2013. Role of hepcidin in the setting of hypoferremia during acute inflammation. *PLoS ONE.* 8:e61050. http://dx.doi.org/10.1371/journal.pone.0061050

Devireddy, L.R., D.O. Hart, D.H. Goetz, and M.R. Green. 2010. A mammalian siderophore synthesized by an enzyme with a bacterial homolog involved in enterobactin production. *Cell.* 141:1006–1017. http://dx.doi.org/10.1016/j.cell.2010.04.040

Drakesmith, H., and A.M. Prentice. 2012. Hepcidin and the iron-infection axis. *Science.* 338:768–772. http://dx.doi.org/10.1126/science.1224577

Fernandez-Pol, J.A. 1978. Isolation and characterization of a siderophore-like growth factor from mutants of SV40-transformed cells adapted to picolinic acid. *Cell.* 14:489–499. http://dx.doi.org/10.1016/0092-8674(78)90235-0

Fischbach, M.A., H.N. Lin, D.R. Liu, and C.T. Walsh. 2006. How pathogenic bacteria evade mammalian sabotage in the battle for iron. *Nat. Chem. Biol.* 2:132–138. http://dx.doi.org/10.1038/nchembio771

Flo, T.H., K.D. Smith, S. Sato, D.J. Rodriguez, M.A. Holmes, R.K. Strong, S. Akira, and A. Aderem. 2004. Lipocalin 2 mediates an innate immune response to bacterial infection by sequestrating iron. *Nature.* 432:917–921. http://dx.doi.org/10.1038/nature03104

Flower, D.R. 2000. Beyond the superfamily: the lipocalin receptors. *Biochim. Biophys. Acta.* 1482:327–336. http://dx.doi.org/10.1016/S0167-4838(00)00169-2

Ganz, T. 2009. Iron in innate immunity: starve the invaders. *Curr. Opin. Immunol.* 21:63–67. http://dx.doi.org/10.1016/j.coi.2009.01.011

Ganz, T., and E. Nemeth. 2012. Hepcidin and iron homeostasis. *Biochim. Biophys. Acta.* 1823:1434–1443. http://dx.doi.org/10.1016/j.bbamcr.2012.01.014

Goetz, D.H., M.A. Holmes, N. Borregaard, M.E. Bluhm, K.N. Raymond, and R.K. Strong. 2002. The neutrophil lipocalin NGAL is a bacteriostatic agent that interferes with siderophore-mediated iron acquisition. *Mol. Cell.* 10:1033–1043. http://dx.doi.org/10.1016/S1097-2765(02)00708-6

Gordon, M.A., D.L. Jack, D.H. Dockrell, M.E. Lee, and R.C. Read. 2005. Gamma interferon enhances internalization and early nonoxidative killing of *Salmonella enterica* serovar Typhimurium by human macrophages and modifies cytokine responses. *Infect. Immun.* 73:3445–3452. http://dx.doi.org/10.1128/IAI.73.6.3445-3452.2005

Guo, K., P. Lukacik, E. Papagrigoriou, M. Meier, W.H. Lee, J. Adamski, and U. Oppermann. 2006. Characterization of human DHRS6, an orphan short chain dehydrogenase/reductase enzyme: a novel, cytosolic type 2 R-beta-hydroxybutyrate dehydrogenase. *J. Biol. Chem.* 281:10291–10297. http://dx.doi.org/10.1074/jbc.M511346200

Hagberg, L., D.E. Briles, and C.S. Edén. 1985. Evidence for separate genetic defects in C3H/HeJ and C3HeB/FeJ mice, that affect susceptibility to gram-negative infections. *J. Immunol.* 134:4118–4122.

Hancock, R.E., K. Hantke, and V. Braun. 1977. Iron transport in *Escherichia coli* K-12. 2,3-Dihydroxybenzoate-promoted iron uptake. *Arch. Microbiol.* 114:231–239. http://dx.doi.org/10.1007/BF00446867

Henderson, J.P., J.R. Crowley, J.S. Pinkner, J.N. Walker, P. Tsukayama, W.E. Stamm, T.M. Hooton, and S.J. Hultgren. 2009. Quantitative metabolomics reveals an epigenetic blueprint for iron acquisition in uropathogenic Escherichia coli. *PLoS Pathog.* 5:e1000305. http://dx.doi.org/10.1371/journal.ppat.1000305

Holmes, M.A., W. Paulsene, X. Jide, C. Ratledge, and R.K. Strong. 2005. Siderocalin (Lcn 2) also binds carboxymycobactins, potentially defending against mycobacterial infections through iron sequestration. *Structure.* 13:29–41. http://dx.doi.org/10.1016/j.str.2004.10.009

John, S.A., and L.A. Garrett-Sinha. 2009. Blimp1: a conserved transcriptional repressor critical for differentiation of many tissues. *Exp. Cell Res.* 315:1077–1084. http://dx.doi.org/10.1016/j.yexcr.2008.11.015

Jones, R.L., C.M. Peterson, R.W. Grady, and A. Cerami. 1980. Low molecular weight iron-binding factor from mammalian tissue that potentiates bacterial growth. *J. Exp. Med.* 151:418–428. http://dx.doi.org/10.1084/jem.151.2.418

Joshi, R., R. Gangabhagirathi, S. Venu, S. Adhikari, and T. Mukherjee. 2012. Antioxidant activity and free radical scavenging reactions of gentisic acid: *in-vitro* and pulse radiolysis studies. *Free Radic. Res.* 46:11–20. http://dx.doi.org/10.3109/10715762.2011.633518

Kawai, T., and S. Akira. 2010. The role of pattern-recognition receptors in innate immunity: update on Toll-like receptors. *Nat. Immunol.* 11:373–384. http://dx.doi.org/10.1038/ni.1863

Kim, P.M., and P.G. Wells. 1996. Phenytoin-initiated hydroxyl radical formation: characterization by enhanced salicylate hydroxylation. *Mol. Pharmacol.* 49:172–181.

Kjeldsen, L., A.H. Johnsen, H. Sengeløv, and N. Borregaard. 1993. Isolation and primary structure of NGAL, a novel protein associated with human neutrophil gelatinase. *J. Biol. Chem.* 268:10425–10432.

Liu, Z., R. Petersen, and L.R. Devireddy. 2013. Impaired neutrophil function in *24p3* null mice contributes to enhanced susceptibility to bacterial infections. *J. Immunol.* 190:4692–4706. http://dx.doi.org/10.4049/jimmunol.1202411

Lord, C.A., D. Savitsky, R. Sitcheran, K. Calame, J.R. Wright, J.P.-Y. Ting, and K.L. Williams. 2009. Blimp-1/PRDM1 mediates transcriptional suppression of the NLR gene NLRP12/Monarch-1. *J. Immunol.* 182:2948–2958. http://dx.doi.org/10.4049/jimmunol.0801692

Lu, Y.C., W.C. Yeh, and P.S. Ohashi. 2008. LPS/TLR4 signal transduction pathway. *Cytokine.* 42:145–151. http://dx.doi.org/10.1016/j.cyto.2008.01.006

Miethke, M., and M.A. Marahiel. 2007. Siderophore-based iron acquisition and pathogen control. *Microbiol. Mol. Biol. Rev.* 71:413–451. http://dx.doi.org/10.1128/MMBR.00012-07

Nairz, M., G. Fritsche, P. Brunner, H. Talasz, K. Hantke, and G. Weiss. 2008. Interferon-gamma limits the availability of iron for intramacrophage *Salmonella typhimurium*. *Eur. J. Immunol.* 38:1923–1936. http://dx.doi.org/10.1002/eji.200738056

Nemeth, E., M.S. Tuttle, J. Powelson, M.B. Vaughn, A. Donovan, D.M. Ward, T. Ganz, and J. Kaplan. 2004. Hepcidin regulates cellular iron efflux by binding to ferroportin and inducing its internalization. *Science.* 306:2090–2093. http://dx.doi.org/10.1126/science.1104742

O'Gorman, S., N.A. Dagenais, M. Qian, and Y. Marchuk. 1997. Protamine-Cre recombinase transgenes efficiently recombine target sequences in the male germ line of mice, but not in embryonic stem cells. *Proc. Natl. Acad. Sci. USA.* 94:14602–14607. http://dx.doi.org/10.1073/pnas.94.26.14602

Oppermann, U., C. Filling, M. Hult, N. Shafqat, X. Wu, M. Lindh, J. Shafqat, E. Nordling, Y. Kallberg, B. Persson, and H. Jörnvall. 2003. Short-chain dehydrogenases/reductases (SDR): the 2002 update. *Chem. Biol. Interact.* 143-144:247–253. http://dx.doi.org/10.1016/S0009-2797(02)00164-3

Park, S.-H., Y.-J. Ko, and C.-K. Kim. 2001. Toxic effects of catechol and 4-cholorbenzoate stresses on bacterial cells. *J. Microbiol.* 39:206–212.

Rathore, K.I., J.L. Berard, A. Redensek, S. Chierzi, R. Lopez-Vales, M. Santos, S. Akira, and S. David. 2011. Lipocalin 2 plays an immunomodulatory role and has detrimental effects after spinal cord injury. *J. Neurosci.* 31:13412–13419. http://dx.doi.org/10.1523/JNEUROSCI.0116-11.2011

Raymond, K.N., E.A. Dertz, and S.S. Kim. 2003. Enterobactin: an archetype for microbial iron transport. *Proc. Natl. Acad. Sci. USA.* 100:3584–3588. http://dx.doi.org/10.1073/pnas.0630018100

Reigstad, C.S., S.J. Hultgren, and J.I. Gordon. 2007. Functional genomic studies of uropathogenic *Escherichia coli* and host urothelial cells when intracellular bacterial communities are assembled. *J. Biol. Chem.* 282:21259–21267. http://dx.doi.org/10.1074/jbc.M611502200

Saiga, H., J. Nishimura, H. Kuwata, M. Okuyama, S. Matsumoto, S. Sato, M. Matsumoto, S. Akira, Y. Yoshikai, K. Honda, et al. 2008. Lipocalin 2-dependent inhibition of mycobacterial growth in alveolar epithelium. *J. Immunol.* 181:8521–8527. http://dx.doi.org/10.4049/jimmunol.181.12.8521

Schaible, U.E., and S.H. Kaufmann. 2004. Iron and microbial infection. *Nat. Rev. Microbiol.* 2:946–953. http://dx.doi.org/10.1038/nrmicro1046

Schroll, A., K. Eller, C. Feistritzer, M. Nairz, T. Sonnweber, P.A. Moser, A.R. Rosenkranz, I. Theurl, and G. Weiss. 2012. Lipocalin-2 ameliorates granulocyte functionality. *Eur. J. Immunol.* 42:3346–3357. http://dx.doi.org/10.1002/eji.201142351

Tili, E., J.J. Michaille, A. Cimino, S. Costinean, C.D. Dumitru, B. Adair, M. Fabbri, H. Alder, C.G. Liu, G.A. Calin, and C.M. Croce. 2007. Modulation of miR-155 and miR-125b levels following lipopolysaccharide/TNF-alpha stimulation and their possible roles in regulating the response to endotoxin shock. *J. Immunol.* 179:5082–5089. http://dx.doi.org/10.4049/jimmunol.179.8.5082

Turlin, E., M. Débarbouillé, K. Augustyniak, A.-M. Gilles, and C. Wandersman. 2013. *Staphylococcus aureus* FepA and FepB proteins drive heme iron utilization in *Escherichia coli*. *PLoS ONE.* 8:e56529. http://dx.doi.org/10.1371/journal.pone.0056529

Vakharia, H.L., and K. Postle. 2002. FepA with globular domain deletions lacks activity. *J. Bacteriol.* 184:5508–5512. http://dx.doi.org/10.1128/JB.184.19.5508-5512.2002

Van Maele, L., C. Carnoy, D. Cayet, P. Songhet, L. Dumoutier, I. Ferrero, L. Janot, F. Erard, J. Bertout, H. Leger, et al. 2010. TLR5 signaling stimulates the innate production of IL-17 and IL-22 by $CD3^{(neg)}CD^{127+}$ immune cells in spleen and mucosa. *J. Immunol.* 185:1177–1185. http://dx.doi.org/10.4049/jimmunol.1000115

van 't Veer, C., P.S. van den Pangaart, M.A. van Zoelen, M. de Kruif, R.S. Birjmohun, E.S. Stroes, A.F. de Vos, and T. van der Poll. 2007. Induction of IRAK-M is associated with lipopolysaccharide tolerance in a human endotoxemia model. *J. Immunol.* 179:7110–7120. http://dx.doi.org/10.4049/jimmunol.179.10.7110

Wessling-Resnick, M. 2010. Iron homeostasis and the inflammatory response. *Annu. Rev. Nutr.* 30:105–122. http://dx.doi.org/10.1146/annurev.nutr.012809.104804

Yang, J., K. Mori, J.-Y. Li, and J. Barasch. 2003. Iron, lipocalin, and kidney epithelia. *Am. J. Physiol. Renal Physiol.* 285:F9–F18.